Crustal evolution in the New England Orogen, Australia: repeated igneous activity and scale of magmatism govern the composition and isotopic character of the continental crust

Siégel C[1,*], Bryan SE[1], Allen CM[1,2], Gust DA[1] and Purdy DJ[3]

[1] School of Earth & Atmospheric Sciences, Science and Engineering Faculty, Queensland University of Technology, 2 George St GPO Box 2434 Brisbane QLD 4001 Australia

[2] Central Analytical Facility, Institute for Future Environments, Queensland University of Technology, 2 George St GPO Box 2434 Brisbane QLD 4001 Australia

[3] Geological Survey of Queensland, PO Box 15261 City East QLD 4002

[*] Now at Deep Earth Imaging, Future Science Platform, Commonwealth Scientific and Industrial Research Organisation, Australian Resources Research Centre, 26 Dick Perry Avenue Kensington WA 6151 Australia

Keywords: crustal evolution; Phanerozoic; zircon; Hf isotope; Tasmanides

ABSTRACT

The generation of continental crust, its bulk composition and temporal evolution provide important records of plate tectonics and associated magma generating processes. However, the long-term integrated effects of repeated magmatic events on crustal growth, composition and differentiation and therefore, on crustal evolution are rarely considered. Here, we examine long-term (~350 Myr) temporal compositional trends of granitic magmatism within a limited (~200 x 100 km) area in the Northern New England Orogen of Queensland, Australia to avoid lateral crustal variations in order to understand how temporal-compositional variations of silicic igneous rocks record crustal evolution. Long-term temporal compositional variations are tracked using whole-rock chemistry, zircon chronochemistry and zircon Hf isotopic compositions. We particularly focus on whole-rock U, Th and K abundances and calculated heat production values as proxies for crustal evolution, and tracking crustal sources involved in granitic magmatism. We identified two major compositional groupings within the study area that were repeatedly produced over

time: Compositional Group 1 comprises voluminous I-type igneous rocks emplaced during the Permo-Carboniferous and Early Cretaceous; and Group 2 represents mainly lower volume A-type igneous rocks of Triassic, Middle Cretaceous and Tertiary age. Importantly, these compositional groupings alternate over the 350 Myr history of granitic magmatism within the study area. Heat production values over time exhibit a zig-zag pattern and mirror zircon Hf isotopic signatures where rocks with elevated heat production values exhibit unradiogenic (crustal) Hf isotopic compositions. We identify the composition of crustal sources, level of the crust undergoing partial melting, scale of magmatism and source crustal volume as important factors in understanding the compositional diversity of silicic igneous rocks. We interpret the two chemical groupings to reflect the following magma generating conditions: Group 1 igneous rocks record large-scale magmatic systems triggered by extensive crustal melting of multiple lower to middle crustal sources which produce more compositionally and isotopically uniform magma compositions that approach bulk crustal compositions. In contrast, Group 2 igneous rocks reflect smaller-scale magmatic systems generated from smaller scale partial melting events of the middle to upper crust that produced A-type magmas. Over the long-term, the successive large-scale magmatic events (recorded by Group 1 igneous rocks) through their concomitant basaltic underplating make the Hf composition of the lower crust more radiogenic, and tend to homogenise the isotopic composition of the continental crust. We consider three important coupled controls: 1) large-scale magmatic systems promote extensive crustal melting potentially blending multiple crustal sources that can also include a significant juvenile source contribution; 2) melt depletion whereby older, and potentially more unradiogenic crustal materials become more refractory; and 3) “crustal jacking” where mantle-derived magmas are added as underplate to the crust (i.e. basification) and can shift older crustal materials to more shallow levels (potentially in concert with erosion and exhumation) and away from zones of crustal melting. Our findings highlight the

importance of integrating the geologic and intrusive history with whole-rock geochemical data and isotopic information, and have direct implications for continental regions that exhibit protracted igneous histories and where isotopic compositions may trend towards more juvenile compositions such as circum-Pacific or retreating accretionary orogens.

INTRODUCTION

For a single parcel of continental crust, the proportion of new crust compared to recycled and differentiated crust can be estimated using U-Pb and Lu-Hf isotopes in zircon from magmatic rocks (e.g. Patchett et al., 2004). Hence, the surface geology can be used to probe the underlying crust. Magmatically–derived detrital zircons are also used to identify major time periods of igneous activity and through interrogation of associated Hf isotopic data to then assess the importance of new crust additions (radiogenic, high positive epsilon values from juvenile magmas recording direct incorporation of basaltic materials into the eventual granite) relative to crustal reworking events (unradiogenic, neutral to negative epsilon values that record ancient material contributions; (Belousova et al., 2010; Cawood et al., 2013; Hawkesworth et al., 2013; Hawkesworth et al., 2016; Condie et al., 2017; Puetz et al., 2017; Condie et al., 2018). Whole rock Sm-Nd isotopes have been used in a similar way (e.g. Wark, 1991; McCulloch et al., 1994; Smith et al., 1996). While new material additions from the mantle are typically basaltic, as expected from experiments of partial melting of mantle peridotite (Yoder & Tilley, 1962), magmas generated during partial melting of crust are intermediate to silicic in composition (Beard & Lofgren, 1991; Patiño Douce & Beard, 1995; Rapp & Watson, 1995). Because the production of abundant new zircon occurs in mostly silicic (granitic/rhyolitic) melts (Siégel et al., 2018a), zircon has become the preferred medium through which we evaluate new crust/recycled crust with Lu-Hf isotopes.

Basaltic magmas are the main vector by which the crust is heated either by underplating or by

direct injection (Huppert & Sparks, 1988). Basalts injected into the crust can have four fates: 1) they can freeze as intrusions that can be later metamorphosed in the crust and perhaps serve as sources of melt themselves; 2) totally cross-cut the crust and erupt as basalts; 3) pond and differentiate to more silicic compositions as observed in layered igneous complexes; or 4) interact and mix with crustal partial melts to produce hybridized intermediate compositions (e.g. Wilcox & Poldervaart, 1958; Huppert et al., 1985; Sparks & Marshall, 1986; Hunter & Sparks, 1987). Granites (rhyolite) can derive from basalt differentiation but the bulk of granite derives from partially melting rocks already resident in the crust and these source rocks range in type from meta-basalts to pelites and graywacke (e.g. Hunter & Sparks, 1987; Chappell & White, 2001; Clemens, 2003).

The physical characteristics of the continental crust and its ability to persist is composition and structure dependent. For example, basaltic underplating thickens and strengthens the crust (Liu & Furlong, 1994), while partial melting and melt extraction removes the more incompatible elements from the lower crust making it more refractory (Green, 1969; Dewey & Windley, 1981). Kemp et al. (2009), for example, suggested that partial melting of tectonically buried continental detritus helped stabilize new continental crust by making granite in a back-arc/retreating arc setting. Put simply, virtually all areas of continental crust and each continental crustal column has a complicated structure and composition built over millions to billions of years in a series of tectonomagmatic events.

Many workers interested in tectonics and continental growth focus on tectonomagmatic events and how the crust might have been affected in that event (e.g., as a crustal recycling or crustal growth event). Here, we are interested in the effects of multiple tectonomagmatic events on a single portion of crust. How does one event affect the rocks produced in succeeding melting events? If we use the same geochemical and isotopic tools on a single

locality, what picture of the crust do we derive, and how does that complement orogenic-scale models (e.g., Kemp et al., 2009; Nelson & Cottle, 2018) where time trends among granite types have been identified and can evolve from S- to I- to A-type, concomitant with changes in zircon initial εHf that are thought to be linked to tectonic evolution? What more do we learn about crustal structure and growth?

We are interested in understanding the evolution of the continental crust as sampled from magmatic rocks (or detritus) at the surface. An important constraint is to have a crustal volume such that the substrate is consistent across the area so that we can minimize the contribution of different crustal substrates in that area/volume, and which is structurally simple so that possible effects of major faulting and duplication and underthrusting can be minimised. Our approach then has been to focus on a relatively structurally simple, 200 by 100 km area in the Northern New England Orogen (Queensland, Australia) where seven age groupings of plutonic and volcanic rocks crop out, the oldest being 350 Ma and the youngest 30 Ma.

The petrogenesis of granitic rocks remains a complex and controversial topic with current debates revolving around fluid absent vs fluid present melting processes (Annen et al., 2006; Jagoutz & Klein, 2018; Clemens et al., 2020; Collins et al., 2020) In this context, we focus on igneous rocks from the higher silica-end of the spectrum because these rocks are more likely to represent relatively uncomplicated crustal melts. By sampling such rocks, we can look at changes of silicic magma composition over time by comparing like-with-like. Any effects from fractional crystallisation processes are evaluated using trace elements. The most sensitive compositional measure of crustal differentiation and evolution in a crustal column are the most incompatible elements, those that move into low-degree partial melts. The high heat producing elements, K, Th and U (or HPE) are chief among these incompatible

elements. HPEs are incompatible elements that are extracted from typically mafic lower crustal regions through partial melting, and then principally transported by silicic magmas and stored in granitic rocks at middle to upper crustal levels (Dewey & Burke, 1973; Dewey & Windley, 1981; Rudnick & Gao, 2003). Repeated magma generation events should therefore concentrate these elements in the upper crust, and this can be expressed by high-heat producing granites, with heat production >5 μWm^{-3} and rarely up to ~10-20 μWm^{-3} (e.g. Middleton, 1979; Förster et al., 1999; McLaren & Powell, 2014; Siegel, 2015). These granites have heat production values far greater than the 2 μWm^{-3} bulk heat production of granitic rocks (Artemieva et al., 2017). HPE enrichment trends in granitic rocks can therefore help map long-term crustal evolution.

GEOLOGICAL BACKGROUND

Geological setting

The study area lies in the northern portion of the New England Orogen (NEO), the youngest and easternmost segment of a large accretionary orogenic system known as the Tasmanides of eastern Australia (Glen, 2005; Rosenbaum, 2018; Fig. 1). The NEO comprises Silurian to Triassic rocks and was developed along the eastern margin of Gondwana. The study area has also been affected by continental rifting and associated seafloor spreading in the Cretaceous as recorded by the Whitsunday Silicic Large Igneous Province (e.g. Bryan et al., 2012), as well as intraplate magmatism during the Tertiary (Johnson et al., 1989). The evidence for long-lived igneous activity exposed within the study area makes it ideal for investigation of long-term Phanerozoic crustal evolution (Fig. 2 and Electronic Appendix 1).

The study area is located between the towns of Bowen and Mackay in eastern Queensland and comprises several igneous and sedimentary terranes (Fig. 2). From west to east, these are: 1) the northern tip of the Permian-Triassic Bowen Basin, which is intruded by Tertiary mafic igneous rocks, 2) the Connors Arch with exposed Permo-Carboniferous and Cretaceous

igneous rocks, 3) the Midgeton Block dominated by Devonian to Permian volcanosedimentary rocks, 4) the Hillsborough Basin, an asymmetric graben filled with Paleogene volcanic and sedimentary rocks, 5) the Airlie Block consisting of Carboniferous to Cretaceous igneous and sedimentary rocks intruded by contemporaneous stocks and dykes, and 6) the Whitsunday Volcanic Province with widespread Cretaceous igneous rocks overlying and intruding Late Triassic granitic basement (Clarke et al., 1971; Ewart et al., 1992; Parianos, 1993; Allen et al., 1997; Bryan et al., 1997; Allen et al., 1998; Bryan et al., 2000).

Igneous activity

At the regional scale, northeastern Australia (Queensland) preserves evidence for prolific magmatism (>175,000 km^2 of exposed igneous rocks or ~10% of the state) with 14 different Phanerozoic tectonomagmatic events (Table 1; Siégel et al., 2012). Half of these occur in the study area. Much of this magmatism has occurred within a 1,000 km wide belt along the eastern margin of Gondwana (Cawood, 1984) and was principally extension-related (Allen et al., 1998; Purdy, 2009; Jell, 2013), but one igneous event occurred during non-collisional orogenesis in the Permo-Triassic (Rosenbaum, 2018). In eastern Queensland and within the study area, the main episodes of magmatism were Late Devonian-Early Carboniferous (360-340 Ma), Late Carboniferous (330-305 Ma), Early Permian (295-270 Ma), Late Permian to mid-Triassic (260-240 Ma), Late Triassic (230-210 Ma), Cretaceous (140-95 Ma) and Late Cretaceous-Tertiary (80-0 Ma, Table 1).

Permo-Carboniferous magmatism developed in a broad back-arc to intraplate setting (Bain & Draper, 1997; Allen et al., 1998; Allen, 2000; Bryan et al., 2001, 2003; Champion & Bultitude, 2013). Early Triassic magmatism temporally overlaps with the contractional Hunter-Bowen Orogeny (Collins, 1991), and has been thought to reflect brief establishment of supra-subduction zone arc magmatism in eastern Queensland, potentially related to

flattening of the subducting slab (Holcombe et al., 1997). This was closely followed by post-orogenic extensional magmatism with A-type characteristics beginning at least by ~230-235 Ma in southeast to east central Queensland (Stephens, 1992; Stephens et al., 1993; Purdy, 2009). Middle Jurassic (~160 Ma) igneous activity is recorded by alkali basalts on the offshore Marion Plateau and silicic tuffs in the Walloon Coal Measures and intrusive rocks of the Maryborough Basin (Kendall, 1992; Isern et al., 2002; Cook et al., 2013; Bryan et al., 2015; Wainman et al., 2015; 2018). A widespread and voluminous (>2.5 million km^3) extensional event that heralded eastern Gondwanan rifting and the opening of the Tasman Sea produced the silicic magmatism of the Whitsunday Silicic Large Igneous Province in the Cretaceous (Bryan et al., 1997; 2000; 2012; Cook et al., 2013). This was followed by bimodal intraplate Tertiary magmatism, with distinctive and strong within-plate geochemical signatures and hotspot-type characteristics (See Johnson et al., 1989 for review).

Nature of crustal basement in the study area

Present-day crustal thickness (Moho depth) is estimated between 33 to 37 km from nearby passive seismic stations west of the study area (Qashqai et al., 2019), and the lithospheric-asthenospheric boundary depth is ca. 80 km (Kennett et al., 2012). This relatively thin lithosphere is the consequence of continental rupture and rifting in the Cretaceous-Tertiary. Seismic sections south of the study area reveal east-dipping reflectors interpreted as crustal-scale thrusts formed during the Permo-Triassic Hunter-Bowen Orogeny (Korsch et al., 1992). The study area abuts the early Paleozoic Charters Towers province to the west where Silurian, Early Ordovician and Late Cambrian igneous rocks are exposed and intrude Late Neoproterozoic to Cambrian metasedimentary rocks (Hutton, 2004). The Proterozoic Georgetown Inlier with crustal Hf model ages of 1880 to 2325 Ma and Mesoproterozoic igneous activity at 1585-1545 Ma (Murgulov et al., 2013) lies to the north of the study area. South of the study area, in the Marlborough province (Fig. 1), a late Neoproterozoic (562 Ma)

ophiolite complex (Princhester Serpentinite) provides the oldest igneous ages identified in the NEO (Bruce & Niu, 2000; Bruce et al., 2000). Proterozoic, Ordovician and Silurian zircon ages (1840, 1400, 600, 475 and 420 Ma) in a garnet-clinopyroxene granulitic xenolith from a Miocene volcanic rock located at the northern tip of the Bowen Basin reveal the presence of Proterozoic to Silurian age lower crust in the region (Allen & Williams, 1998).

Isotopic evolution in the study area

At a variety of spatial and temporal-scales, Sm-Nd, Sr whole-rock, and zircon Hf isotope analyses from igneous rocks reveal a long-term trend towards more isotopically juvenile compositions across the Tasmanides (Allen et al., 1997; Allen, 2000; Kemp et al., 2009; Collins et al., 2011; Siégel et al., 2018b). This temporal isotopic trend has been explained by: 1) the long-term addition of large-volumes of mafic igneous rock to the lower crust over ~100 to 200 Myr and 2) the removal of older crust by thermal erosion in a back-arc environment and/or mechanical erosion during subduction (Collins et al, 2011).

A long-term temporal change in the composition of granitic rocks is also recognised with a shift from S- to I- to A-type, particularly in the neighbouring and older Lachlan Orogen (Kemp et al., 2009). Concomitant with this compositional shift was a change in igneous volumes with A-type igneous rocks being volumetrically minor (Kemp et al., 2009). Kemp et al. (2009) linked this long-term trend to increasing proportions of juvenile mantle magmas in the I-type igneous rocks. Time gaps separating the compositionally different igneous events correspond to a change of tectonic environment, such that tectonic setting controls the proportions of juvenile materials involved in magma generation, and hence the shift of magma composition from S- to I-type (Kemp et al., 2009).

A similar temporal change in isotopic composition is broadly observed for the southern NEO where many Early Permian (295–288 Ma) granitoids are S-type and are followed by Late

Permian to Middle Triassic (260–235 Ma) igneous rocks that are typically I-type in composition (Kemp et al., 2009; Shaw et al., 2011). However, in the northern NEO and surrounding the study area, Permian magmatism (300–260 Ma) is dominated by I-type granitoids. The volumetrically minor S-type and A-type granitoids are broadly coeval (290–260 Ma) but spatially separate and are most abundant in northern Queensland (Champion & Bultitude, 2013; Rosenbaum, 2018). Consequently, while in some parts of the Tasmanides S- and I-type magmas may be separated in time, in other parts, the generation of S-, I- and A-type igneous rocks appears to be controlled by the particular geology of the source terrane, rather than any temporal evolution including change of tectonic setting/stress regime (for example, see figure 6.18 of Champion & Bultitude, 2013).

METHODS

To evaluate the evolution of continental crust, we investigated long-term compositional and isotopic trends in a volume of crust that has experienced numerous magmatic events but is small enough to negate the effects of large-scale structural changes in basement. Surface areas of igneous rocks are used to approximate igneous volumes, and changes in HPE concentrations in silicic igneous rocks are used as a proxy for crustal differentiation.

Ninety-eight samples were collected that provide sufficient spatial and temporal coverage of all igneous events within the study area (Fig. 2). Sample collection focussed on silicic (SiO_2 >70 wt%) igneous rocks (extrusive and intrusive) of all ages to achieve a well-constrained temporal spectrum for the silicic endmember of all igneous rocks (potentially minimum melts of crustal sources). Most samples studied are biotite- and/or hornblende-bearing granitic rocks. Additionally, flow-banded rhyolite, ignimbrite and obsidian form part of the dataset to capture the compositional characteristics of the youngest and shallowest exposed levels.

Quantitative modal mineralogies were determined by point counting (500 points per sample).

REE-, U- and Th-bearing accessory minerals were identified using scanning electron microscopy and magnetic susceptibilities were measured in the field. Seventy-six samples were selected for whole-rock chemistry with major and trace elements analysed by XRF and ICP-MS, respectively. All analyses are normalised to 100% on an anhydrous basis and are reported in Electronic Appendix 2. Sixteen samples were then selected for zircon U-Pb dating and zircon Hf isotopic analysis. Zircons were imaged by cathodoluminescence (CL) prior analysis. Approximately 40 to 70 analyses per sample were acquired for U-Pb dating and trace elements. Hf isotope analyses were performed on different locations than age analyses, but on the same grain and within zones of similar CL response. Only grains providing emplacement ages were analysed for Hf isotopes. Zircon ages and Hf isotopic data are reported in Electronic Appendix 3 and the accuracy of each analytical session is summarised in Electronic Appendix 4. Further details on rock sample preparation, data integrity, analytical details for whole-chemistry, point counting, SEM-EDS analyses, zircon chronochemistry and Hf isotope analysis are given in Electronic Appendix 4.

RESULTS

U-Pb age data and emplacement ages

We follow the approach of Siégel et al. (2018a) to determine emplacement ages as explained in Electronic Appendix 4. The new U-Pb emplacement ages include three Early Carboniferous, three Late Carboniferous, two Permian and three Early Cretaceous intrusions, as well as two granitic rocks and one rhyolite of Middle Triassic age, and one intrusion and one obsidian of Tertiary (latest Eocene) age (Table 2, 4). Thus, the emplacement ages for the sixteen rock samples dated correspond to six of the seven identified tectonomagmatic events (Tables 1-2); they highlight good temporal coverage of our dataset. The proportion of zircon inheritance as well as the diversity of inherited ages appear to decrease over time being greater in the Permo-Carboniferous samples compared to the Middle Triassic and younger

igneous rocks (Table 2).

Mineralogical and compositional groupings

Two distinct age-interspersed groups are recognised based on mineralogy and whole-rock composition of the studied silicic igneous rocks (Table 3). Similar trends are observed using all compiled silicic igneous rocks in the study area (n=1186; see Siegel, 2015; data available upon request). Group 1 exhibits similar mineralogical and compositional characteristics regardless of age, while Group 2 show distinctive mineralogical and compositional characteristics for each age suite, but collectively remain distinct from Group 1 igneous rocks. Group 1 comprises Permo-Carboniferous and Early Cretaceous silicic igneous rocks that are volumetrically dominant within the study area (Fig. 2), typically forming individual exposures >1,000 km^2 (Table 4); they are also the dominant-aged igneous rocks at the regional scale in Queensland (Jell, 2013). The Group 1 rocks have a wide range of magnetic susceptibility (0 to ~$20x10^{-3}$ SI), and a high proportion of plagioclase and mafic minerals (e.g. biotite and hornblende) where biotite has elevated Mg# (20-50). Ca-rich plagioclase (up to An_{60}) occurring as resorbed cores and with oscillatory zoned rims are distinctive in the Group 1 rocks, and potassic alkali-feldspars are also present (Table 3).

Group 2 comprises Middle Triassic, Middle Cretaceous and Tertiary silicic igneous rocks. The Group 2 silicic igneous rocks are volumetrically minor, forming individual exposures <1,000 km^2, although Middle Cretaceous volcanic rocks are more abundant at the regional scale (e.g. Bryan et al., 2012). The Group 2 igneous rocks generally have very low magnetic susceptibilities (except for the Middle Cretaceous) likely due to lower abundance of magnetite, a high proportion of alkali-feldspar, and low abundances of plagioclase (which also lacks resorbed, high-An cores) and mafic minerals. Mineral compositions are distinctive in Group 2 with low Mg# (<30) in biotite, and high Na-contents in plagioclase (<An_{30}) and alkali-feldspars (Table 3). The low magnetic susceptibility and iron-rich biotite suggest the

Group 2 rocks derive from more reduced magmas.

Differences between the two groups extend to the accessory mineralogy. Common accessory minerals in Group 1 are thorite/huttonite, monazite, cheralite, allanite, xenotime, apatite, titanite, and zircon, whereas exotic minerals such as Parisite-Nd, samarskite, uranoan Zr-rich thoriopyrochlore, fluocerite, chevkinite, and fluorite are distinctive in Group 2. U and Th-bearing accessory phases are hosted in both early- and late-crystallising minerals for Group 1 and Group 2 igneous rocks.

All samples plot in the calc-alkaline and sub-alkaline fields of Irvine and Baragar (1971). Most samples plot in the granodiorite, monzogranite, syenogranite, and alkali-feldspar granite fields, with Group 2 igneous rocks exhibiting more alkali-rich compositions (Fig. 3a). Group 1 igneous rocks dominantly plot in the magnesian and calcic to calc-alkalic fields of Frost et al. (2001) whereas Group 2 igneous rocks essentially plot in the ferroan and alkali-calcic to alkali fields (Figs 3b-c). The Alumina Saturation Index (ASI) for the silicic igneous rocks ranges from 0.9 to 1.3 and most igneous rocks plot at the boundary between metaluminous and peraluminous compositions. A few Tertiary samples plot in the peralkaline field (Fig. 3d). Furthermore, many Group 2 rocks plot in the A-type field of Whalen et al. (1987), whereas Group 1 igneous rocks plot dominantly in the combined I-S-type field (Fig. 3e). Group 1 and Group 2 silicic igneous rocks exhibit different trace-element characteristics: Group 2 exhibit higher MREE, HREE, Zr, Hf, and lower Eu/Eu*, Ba, Sr, Ti and Sr/Y in comparison to Group 1 (Fig. 3f; Table 3). The Tertiary igneous rocks of Group 2 are the most strikingly different, with pronounced Ba depletion and significant enrichments in Cs, Nb, Ta, REE, Zr and Hf compared to bulk continental crust (Fig. 3f). Zircon saturation temperature calculations based on whole-rock chemistry (Watson & Harrison, 1983) also differ for both groups (Group 2: >800°C; Group 1: <800°C; Table 3). This difference mostly reflects higher Zr contents for the Group 2 suite (Fig. 3e). Of note is that the Zr saturation temperatures for

Tertiary and Middle Triassic igneous rocks of Group 2 are in the range 850-920°C, which is higher than reported for most granitic rocks (e.g., Miller et al. 2003; Siegel et al., 2018a). Such temperature does not reflect the temperature of the magma but rather the temperature at which the magma is saturated and starts crystallising zircons.

In summary, Group 1 igneous rocks are I-type based on their metaluminous, magnesian, and hornblende-bearing character. Group 2 igneous rocks are A-types as shown by their ferroan, alkali-calcic to alkalic whole-rock chemistry, high Ga/Al ratios, low Mg# in biotite, low anorthite contents in plagioclase (measured from semi-quantitative SEM-EDS analyses), occurrence of Na-rich plagioclase and accessory phases such as chevkinite and fluorite in Tertiary igneous rocks, and the coexistence of fayalite and quartz in the Tertiary BEL-02 obsidian (see also Bonin, 2007).

Composition and heat-production trends over time

Several key temporal trends are observed in the whole rock (mostly granite) data. Most Group 1 igneous rocks have U, Ta, Nb, Hf to Sm and Y contents lower than upper continental crust values (Fig. 3f), while Group 2 igneous rocks have greater contents. Ba abundances become more depleted over time with a significant relative depletion for Group 2 igneous rocks.

Heat production over time (~ 320 myrs) shows no systematic trend/vector. Rather, U, Th and K_2O contents, as well as heat production, vary between each tectonomagmatic event (Fig. 4). Heat production is moderately high in Early Carboniferous granites (~2 μWm^{-3}) but less in the Late Carboniferous (average value of ~1 μWm^{-3}). Average heat production increases for the Middle Triassic intrusions, with values ranging between ~1.8 to 3.8 μWm^{-3}. Heat production values for Early Cretaceous granitoids are lower, before increasing in the Middle Cretaceous to the Tertiary, reaching values of 2.8 to 3.6 μWm^{-3}. Two specific outliers in the

dataset (CHR-01 and SCR-01) are interpreted as highly fractionated rocks based on field, geophysical and geochemical data (e.g. high radiometric response, elevated Rb/Sr) (Fig. 4b). Another outlier (MH-01) does not, however, possess elevated Rb/Sr and fractionation is thus an unlikely explanation for this unit.

Zircon morphologies, textures and compositions

Zircons from Group 1 igneous rocks (Cretaceous, Permian and late Carboniferous) exhibit a greater diversity of morphologies and textures in comparison to zircons from Group 2 rocks (Tertiary and Middle Triassic). Morphologies for the Group 1 zircons range from acicular, equant, stubby and prismatic as highlighted by the greater range of aspect ratio: ~1 to 6 vs ~1 to 3 for Group 2 zircons. Textures revealed by cathodoluminescence tend to be more complex for Group 1 zircons with strong oscillatory zoning and internal structure and greater variability within individual rock samples. In contrast, zircons from Group 2 show less internal structure and form a more homogeneous population (e.g., Tertiary zircons have faint cathodoluminescence response and exhibit sector zoning; Electronic Appendix 5).

Zircons from Group 2 rocks, and some from Group 1 Early Carboniferous granitoids, have flat REE patterns (high Dy_N/Lu_N; >0.2), a restricted range of Ce/Ce* < 220, Eu/Eu*<0.30, and low Th/U values (<1) (Electronic Appendix 6). Zircons from Group 1 igneous rocks have steep REE patterns (Dy_N/Lu_N <0.2), a wide range of Ce/Ce* >300 and Eu/Eu*>0.30, and higher Th/U (up to 2.5). Low Ce/Ce* (small positive Ce anomalies) and Eu/Eu* (large negative Eu anomalies) for zircons from Group 2 suggest the zircons derive from reduced magmas, whereas zircons from Group 1 crystallised in relatively more oxidised magmatic environments (Trail et al., 2012). This is consistent with the contrasting magnetic susceptibility and biotite composition between the two groups (Table 3). Th and U contents in zircons from both groups are commonly <0.1 wt%, and not anomalous (Harley & Kelly, 2007). Furthermore, U and Th contents are not preferentially stored in either zircon cores or

zircon rims. Overall, xenocrystic zircons have similar or lower U and Th contents to emplacement age zircons.

Hf isotopes

Hf isotopes from zircons of Group 1 exhibit a greater variability (ƐHf= -7 to +11) in comparison to zircons from Group 2 (ƐHf= +0 to +8). Hf isotopic compositions for zircons of Group 2 igneous rocks as well as the most radiogenic (more positive) Carboniferous zircons (MH-01, BN-02, HECT-02 and VIO-01) align along a broad crustal evolution curve represented by model ages of 650 to 1000 Ma (Fig. 5). Overall, Hf isotopes in zircons reveal three main signatures: 1) unradiogenic (more crustal-like or negative) Hf isotopic compositions for the Early Carboniferous CUR-02 and CAP-04 granites and Permian igneous rocks with ƐHf= -7 to +1 and Precambrian Hf model ages (~1180-1400 Ma); 2) moderately unradiogenic to juvenile signatures for the Early Carboniferous MH-01, Late Carboniferous, Middle Triassic and Tertiary igneous rocks (ƐHf= 0 to +8; Hf model ages of ~650-1000 Ma); and 3) highly positive and juvenile isotopic compositions for the Cretaceous (ƐHf= +7 to +11; Hf model ages of ~430-580 Ma) (Fig. 5). Importantly, a long-term trend towards more radiogenic and isotopically more uniform signatures and decreasing model ages is evident in the Hf isotopic data (Fig. 5a). Whole-rock Nd and Sr isotopes define a similar trend (Fig. 5b, c), noting that differences between the Hf and Nd isotope spreads for the Permian and Triassic essentially relate to the bulk-rock type analysed (e.g. basalt versus highly silicic; the former being more juvenile). Hf isotopes also mirror heat production values for the majority of igneous rocks studied here (Fig. 6). The samples with more crustal epsilon Hf also have greater HPE, although this is less strongly developed in the Middle Triassic igneous rocks.

DISCUSSION

Repeated continental magmatism over long timescales (10^7-10^8 yrs) has the potential to drive crustal differentiation. The compositional characteristics of one igneous event may be

impacted by previous magmatic events. Past studies at regional or orogen scales have highlighted long-term compositional and isotopic trends where upper crustal granitic magmas change from S- to I- to A-type and where zircon Hf isotopic compositions also become more radiogenic over time (Kemp et al., 2009).

Results from this study of long-term granitic magmatism reveal two distinct compositional groupings that correspond to I- and A-type affinities, but rather than following a unidirectional change over time from I- to A-type, alternations between the two compositional groups occur. Here, we first discuss the origins of the two compositional groupings (I- and A-type), and then causes for their alternation through time in the study area. We then evaluate what the integrated effects of the repeated magmatic events have been on: a) the subsequent igneous event and compositions, b) crustal source composition, and c) crustal differentiation and crustal evolution in this 200 by 100 km patch of crust.

Origin of compositional groups and changes

Two broad controls exist for generating the differences between the two granitoid compositional groups identified in the study area: 1) partial melting of different crustal sources, and 2) magmatic processes such as differing extents of fractional crystallisation. We also discuss below the 'scale of the magmatic system' involving the degree of crustal partial melting and the volume of rock subjected to partial melting as a potential factor in generating these compositional differences, while recognising limitations on knowing magma volumes.

Magmatic differentiation processes

We have used HPE as a monitor of crustal differentiation. U- and Th-bearing accessory phases that primarily control HPE in granitic rocks are hosted in both early- and late-crystallising minerals within the studied silicic igneous rocks suggesting that U- and Th-enrichment can be either or both source- and fractional crystallisation-controlled. Within each

tectonomagmatic event, no correlation exists between HPE and Rb/Sr and/or Eu/Eu* as fractionation indices. Some Middle Triassic and Tertiary igneous rocks have high HPE and high Rb/Sr whereas others have similar HPE but low Rb/Sr indicating that HPE concentration is not primarily fractionation-controlled (Fig. 4b). As our sampling targeted silicic igneous rocks with SiO_2 >70 wt%, we consider that these rocks are minimum melts with their associated HPE contents, and that only a few are modified by fractionation.

Crustal source control

The heat production pattern over time mirrors (i.e. is opposite in trend to) the zircon epsilon Hf values (Fig. 6) suggesting that crustal source compositions strongly impact the heat production capacity of their partial melts. Hf model ages and inheritance, as indicated by the ages of zircon cores, indicate partial melting of a significant amount of Precambrian crust (Figs 5-6). Precambrian crust in Australia is generally high-heat-producing (Sandiford et al., 2001; McLaren & Powell, 2014) and reworking of material of this age (as shown by Hf isotopes) would therefore increase the heat production potential of igneous rocks. There is an outstanding exception in that the Middle Triassic igneous rocks are more isotopically juvenile yet have a relatively high heat-producing character (Fig. 6). In this case, and considering the Hf data, we interpret the anomalous Middle Triassic igneous rocks to be low degree partial melts of Phanerozoic granitic rocks enriched in heat-producing source materials (e.g., K, U and Th).

The repeated production of compositionally similar granites, in the same area at different times, suggests the mineralogical and compositional differences of Group 1 and Group 2 granites (Table 3) reflect two distinct source regions in the Bowen-Mackay area. Given that the compositional variations occur in a ~200 x 100 km area, these different source regions are likely to be in a vertical arrangement, and thus may reflect differing depths of crustal partial melting. The relative lack of zircon inheritance and absence of S-type granitic rocks in the

study area reinforce the interpretation that the crust involved in partial melting is principally igneous in type.

Group 1 crustal sources. Based on the relatively low abundance of xenocrystic zircons, dominant metaluminous compositions and mafic mineralogies (biotite+/-hornblende), the crustal source for Group 1 I-type igneous rocks is interpreted to be mafic igneous or meta-igneous in origin (Chappell & White, 1974, 2001). Comparison of geochemical data with partial melt experiments suggest that source rocks for Group 1 igneous rocks are amphibolite with plagioclase as the main Al-bearing mineral phase, rather than garnet (Fig. 7). Indeed, partial melting in presence of garnet (higher pressure/deeper) would lead towards more trondhjemitic magmas (e.g. Rapp et al., 1991). Here, we interpret Group 1 igneous rocks to derive from high-temperature dehydration melting of biotite and amphibole hosted in amphibolite facies meta-igneous rocks as the result of the intrusion of mantle-derived magmas into the crust, and importantly, any mantle contribution to the silicic magmas is not contemporaneous.

Group 2 crustal sources. A-type granites, in general, may derive by fractionation of transitional to alkaline mafic to intermediate, mantle-derived magmas (Loiselle & Wones, 1979; Bonin, 2007) or by partial melting of a dry and refractory granulitic lower crust (Clemens et al., 1986; Johannes & Holtz, 1996), an alkali-metasomatized crust (Martin, 2006), a calc-alkaline tonalite or granodiorite (Creaser et al., 1991; Patiño Douce, 1997) or sources similar to ocean island basalt compositions (Eby, 1992). As evaluated above, fractional crystallisation is unlikely to be a dominant process in producing the Group 2 A-type igneous rocks as the granites lack geochemical indices for extensive fractionation (e.g., elevated Rb/Sr and Eu anomalies) and the basaltic parental magmas are generally depleted in HPE (Wollenberg & Smith, 1987). The Group 2 A-type igneous rocks of the Bowen-Mackay

area are enriched in HPE, ruling out LIL- (and HPE-) depleted lower crustal granulites and underplated basalts as sources. An alkali-metasomatized crustal source (Martin, 2006) is also ruled out as it would have led to U-enrichment and a decoupling between U and Th, due to U mobility and Th immobility (McCulloch & Gamble, 1991), which is not what is observed in the studied A-type rocks. The most likely source then of Group 2 A-type granites, consistent with their HPE enrichment, trace element and isotopic characteristics and the results of melting experiments (Fig. 7), is a magnesian calc-alkaline (I-type) tonalite or granodiorite. Such rocks are more enriched in HPE than basalt (Wollenberg & Smith, 1987), and upon melting will yield U, Th and K enriched, high-silica magmas. Notable features of the A-type igneous rocks, as particularly observed in the Tertiary silicic igneous rocks, are positive Nb and Ta anomalies and enrichment of high-field strength elements (HFSE) (Fig. 3f). The generation of positive Nb and Ta anomalies from sources with potentially significant negative Nb and Ta anomalies requires the high-temperature dissolution of Nb- and Ta- bearing accessory phases such as titanite and rutile (Creaser et al., 1991). Formation of Group 2 A-type igneous rocks therefore requires a significant heat supply to partially melt those less fertile sources. This likely occurs via the ascent of mantle-derived magmas to shallower crustal levels, hence providing direct heat-transfer (Patiño Douce, 1997).

Ages of crustal sources. Now that we have discussed how whole-rock geochemistry coupled with melting experiment constraints help resolve compositional differences in the sources for the Group 1 and 2 igneous rocks, we focus on zircon Hf isotopic data to derive information on the relative ages of the crustal sources. Hf model ages are useful tools to unravel the broad nature and age of the crust but accuracy is limited by assumptions about the $^{176}Lu/^{177}Hf$ of the protolith, as well as the assumption of a single, strongly depleted mantle source (Kemp & Hawkesworth, 2014; Vervoort & Kemp, 2016) and the lack of contemporaneous magma mixing. Two-stage model ages calculated using various Lu/Hf of

the crust (Condie et al., 2011; Chauvel et al., 2014), depleted mantle models (Griffin et al., 2000; Dhuime et al., 2011; Iizuka et al., 2013) and λ^{176}Lu decay constants (Blichert-Toft & Albarède, 1997; Scherer et al., 2001; Söderlund et al., 2004) result in age differences of ~400 Myr for our data and thus uncertainties for this dataset could be this great.

Three main isotopic signatures exist in the Hf isotope sample suite which could be interpreted by the presence of three crustal sources of different ages (Fig. 5). However, we suggest that several source components must have been involved in any one granite generation because: 1) each sample exhibits a range of ƐHf, corresponding to a span of >100 Myr model ages, and 2) model ages do not necessarily overlap with periods of known igneous activity (see dark-grey bands in Fig. 5 representing crustal evolution curves).

The highly silicic and unfractionated composition of most samples indicates that they acquired their composition through crustal partial melting. There is little evidence for any contemporaneous mantle-derived materials to have substantially contributed to silicic magma volume and chemical character. However, non-contemporaneous mantle-derived basaltic underplates and basalt emplaced in the lower to middle crust during previous magmatic events are potential and likely crustal magma sources for the granites.

To further resolve the potential crustal source characteristics involved for each tectonomagmatic event (Table 1) and to establish a crustal column inventory, we combine: 1) Hf model ages, 2) zircon inheritance characteristics, 3) geochemical information (HPE and silica contents), and 4) constraints from the regional geology (Table 5) including ages of known igneous basement rocks within and surrounding the study area (grey crustal evolution curves in Fig. 5; Table 5), to develop Figure 8 which tries to cast the depths and mixture of potential sources, with real constraints from Hf isotopes in terms of proportional mixes (mass balance). Key findings from integrating these different datasets are: 1) the recognition of

different type/composition of crustal sources for Group 1 and Group 2 igneous rocks reflecting partial melting of contrasting crustal levels; 2) the more voluminous character of Group 1 igneous rocks versus Group 2; 3) the greater diversity of crustal source ages for Group 1 igneous rocks in contrast to Group 2; and 4) the younging of those crustal sources over time (Fig. 8).

Scale of magmatism controls compositional groupings: a crustal inventory

Figure 8 captures our main database and interpretation for the evolving structure of the Mackay-Bowen crustal column. A feature of the Group 1 igneous rocks is their mineralogical and compositional homogeneity (Fig. 3) despite being produced at different times from the Carboniferous to Cretaceous. The Group 1 plutons have large exposed surface areas (Table 4), which we assume reflects the generation of large magma volumes, and given our arguments above, reflects a similar degree of partial melting of a large volume of source rock. A caveat to this logic is that although within the study area Cretaceous magmatism appears to be relatively low-volume (Table 4), at the regional scale and in proximity to the study area, igneous volumes are immense (Bryan et al., 2012) and the largest for all the igneous events studied here. In contrast, the Group 2 Tertiary silicic igneous rocks are volumetrically minor, both at a local scale and regionally, across eastern Australia (see Table 4 and Johnson et al., 1989).

We suggest two main source rock-types for the two groups: 1) large-scale magmatic systems producing I-type igneous rocks of Group 1 by partial melting of predominantly mafic igneous sources resident in the crust in the Late Carboniferous, Permian and Early Cretaceous igneous events; and 2) smaller-scale magmatic systems producing A-type igneous rocks of Group 2 during the Middle Triassic, Middle Cretaceous and Tertiary igneous events (Fig. 6) that result from partial melting of tonalitic to intermediate metaigneous rocks. Large-scale crustal partial melting systems, as expressed by the tectonomagmatic events with cumulative exposed

surface areas of igneous rock >61% of the study area (Table 4) were more energetic because they were driven by higher rates and larger volumes of contemporaneous basaltic underplating (as supported by elevated seismic velocities in the lower crust; see Electronic Appendix 7) and intrusion, triggering extensive partial melting of potentially multiple crustal sources in the lower to middle crust. The resulting magma compositions thus approach the composition of the bulk continental crust (Rudnick & Gao, 2003) and explains the relatively flat trace element patterns in multi-element plots (Fig. 3f). The diversity of Hf isotopes of Group 1 igneous rocks relate to the larger number of crustal source materials of different ages (various crustal residence times) being involved in partial melting (Fig. 8).

In contrast, smaller-scale systems such as represented by Group 2 igneous rocks representing cumulative surface exposure areas <10% of the study area (Table 4), are less energetic and involve more localised partial melting of more restricted crustal sources (Table 5). The uniformity of Hf isotopes for Group 2 A-type igneous rocks is explained by: 1) partial melting of intermediate to upper crustal level sources with similar Hf model ages (e.g. Early, Late Carboniferous or Middle Triassic; T_{2DM}=650-1000 Ma), and 2) elevated temperature of melting as suggested by the absence of restitic (inherited) zircons. We interpret the isotopic signatures for Tertiary A-type igneous rocks do not directly reflect partial melting of Proterozoic crustal material, but are likely inherited from their immediate source (Carboniferous or Middle Triassic granitic rocks, which had previously been generated by partial melting of Proterozoic crustal materials). The predominance of these model ages (650-1000 Ma) in the study area is interpreted to relate to large-scale magmatism in the Carboniferous, which reworked Cambro-Silurian and Precambrian crust to generate abundant granitoids.

Crustal differentiation

Over this long-lived history, the scale and volume of exposed granitic rocks in the upper crust

indicate the continental crust at this location has undergone substantial differentiation; the corollary is that middle and lower crustal melt source reservoirs have been depleted. The relative enrichment of incompatible elements in the upper crust is indicated by the long-term trends for heat production values and incompatible element enrichments being highest in the Tertiary silicic igneous rocks (Figs 3-4). Coupled with this upper crustal enrichment is the indication that the lower crust has become more mafic and juvenile in Nd and Hf isotopic composition over time ("basification" of Allen et al., 1997) in the form of igneous, then metaigneous mafic rocks that have become available as crustal growth has occurred. Evidence for this is the long-term trend towards more juvenile isotopic signatures from the Early Carboniferous to the Early Cretaceous (Fig. 5). Seismic data coupled with xenolith information for neighbouring regions (Electronic Appendix 7; Griffin et al., 1987; Collins, 1988) indicate the existence of both a layered and mafic lower crust that occurs regionally and consists of mafic granulites, i.e. basaltic intrusions that were previously added to the lower crust and underwent high grade metamorphism..

The combination of heat production values with the zircon Hf isotopic data highlight two important features (Fig. 6). First, heat production mirrors zircon Hf isotopes where the more unradiogenic granitic rocks derived from Precambrian sources have the higher heat production values. Second, that over time, these Precambrian sources become less prominent (Table 5; Figs 5&8). The apparent loss of radiogenic isotopic signatures within a discrete segment of an orogen over time, rather than resulting from the physical loss and removal of unradiogenic crust as one mechanism suggested by Collins et al. (2011), may result from the combined effects of: 1) melt depletion making those crustal materials more refractory, 2) "crustal jacking" whereby basaltic underplating (that may be coupled with surface uplift and exhumation; e.g. Roy et al., 2004) drives pre-existing old crust to higher/cooler structural levels, and 3) underplating and crustal invasion by mantle-derived magmas forming dyke-sill

networks through the crust that begin to volumetrically overwhelm the pre-existing lower crust (Fig. 10). Any of these three mechanisms, depending on the locus of melting within the evolving crustal profile, account for why older sources may "reappear" over time, which is what is observed with the Tertiary igneous rocks (Group 2). In this case, we argue that the rise of mantle-derived magmas to higher structural levels triggered partial melting of tonalites/granodiorites that were formed in previous tectonomagmatic events, explaining the more unradiogenic isotopic characteristics of the Tertiary silicic igneous rocks (Fig. 5). For the Tertiary igneous rocks, we exclude Precambrian crust as potential sources because Tertiary rocks are more enriched in HPE in comparison to the earlier Carboniferous ones that have similar Hf isotopic signature. While remelting the same source will lead to similar isotopic signatures, it would also lead to a decrease in incompatible elements including U, Th and K, the opposite to what is observed. A key conclusion, then, of our long-term perspective of granitic magmatism is that over time, some crustal rocks simply become unavailable as magmatic sources (Table 5; Figs 5&8). This does not necessarily mean those crustal sources have been physically removed from that crustal section by some large-scale tectonic process. In particular, we argue that Precambrian crust is present in the crustal profile in the Tertiary as evidenced by the occurrence of Proterozoic zircons in granulite xenoliths from Miocene volcanic rocks in the northern tip of the Bowen Basin (Allen & Williams, 1998). Focusing solely on one igneous suite can thus lead to a biased picture of the age, composition and evolution of the crustal profile in that region because some sources may no longer undergo partial melting. Studying intrusions of different ages, like we do here, provides better context, and helps to establish the persistence (or not) of crustal sources (Hf isotope compositions lie on the same crustal evolution curve, or discrete ones; Fig. 5), thereby showing how past crustal sources/products can impact on younger igneous products.

The long-lived and highly productive magmatic history of the Bowen-Mackay area reflects

numerous crustal partial melting events which requires a crustal column that remained relatively fertile. Melt fraction removal inherently reduces future melt fertility. Fertility can be enhanced by volatile-fluxing (hydration) in active supra-subduction zone settings (Hyndman et al., 2005; Tatsumi, 2005; Collins et al., 2016) but our study area lacks subduction zone arc magmatism and is considered remote from paleosubduction zones. As an alternative, we suggest that the addition of mantle-derived magmas associated with major crustal melting events first added sufficient heat to cause partial melting (e.g. Huppert & Sparks, 1988; Annen et al., 2006), but then these rocks became potential melt sources through metamorphism, and have thus been fundamental to maintaining melt fertility in this crustal column.

Crustal evolution

Long-term compositional trends for zircon Hf isotopic signatures indicate a broad trend towards more juvenile isotopic signatures from the Early Carboniferous to the Early Cretaceous, followed by a return to more unradiogenic compositions in the Tertiary (Figs 5-6). Importantly, crustal sources involved in partial melting became younger in successive melting events (Table 5; Figs 5&8). Older crust, in particular, Precambrian Georgetown- and Musgrave-type crustal materials, were not participating at the source of melt generation after the Permian (Figs 5-6). This observation is in agreement with Allen et al. (1997) and Allen (2000), in which significant addition of mantle-derived magmas into the crust in the Late Carboniferous-Early Permian was interpreted to have strongly affected the composition and character of the lower crust.

At the scale of this study, the general trend in crustal evolution towards more juvenile isotopic compositions is consistent with isotopic trends observed at larger scales in the neighbouring Thomson and Lachlan orogens (Fig 8; Kemp et al., 2009; Cross et al., 2018; Siégel et al., 2018b). At the orogen-scale, this trend has been coupled with a temporal shift

from S- to I- to A-type granitic compositions and changes in tectonic setting (Kemp et al., (2009). While the general isotopic trend is observed in our study area, including the observation of decreasing old crust participation in melting, the granite compositional trend is not like the one reported by Kemp et al. (2009). No S-type granites occur in the study area, and the Tertiary A-type igneous rocks have more crustal Hf isotopic signatures in comparison to the preceding highly juvenile Cretaceous I-type igneous rocks; this contrasts with the compositional trends observed in the southern part of the Tasmanides (Kemp et al., 2009). This study cannot simply tie changes of granite type to changes of tectonic setting as interpreted by Kemp et al. (2009) in their transect across the southern portion of the orogen. When other data from the Lachlan Orogen (Shaw et al., 2011) are included, it also reveals a reversal to more isotopically unradiogenic compositions (Fig. 9). In the Lachlan Orogen case, that reversal may relate to lateral crustal variation as the younger and more unradiogenic Carboniferous Bathurst Granite (Shaw et al., 2011) is located ~150 km north of the other samples used in the Kemp et al. (2009) study.

The dominant orogen-scale trend towards more isotopically juvenile signatures is coupled with less isotopic diversity at the local scale (Fig. 5). In particular, for the Bowen-Mackay study area, Permo-Carboniferous igneous rocks exhibit a variation of >15 ƐHf units whereas Early Cretaceous igneous rocks are characterised by a much smaller range (<5 ƐHf units) (Fig. 5). We relate the more isotopically juvenile character of the crust and the loss of isotopic diversity over time to result from the repeated development of large-scale magmatic systems driven by the delivery of basalt into the crust. The combination of basaltic magma addition to the lower crust and partial melting of multiple crustal sources homogenises the long-term crustal isotopic composition of extracted granitic magmas while leading to lower crustal source regions with a more isotopically uniform character and composition resembling the bulk continental crust. Chief among these are the Middle Cretaceous

Whitsunday rocks which have an outstandingly juvenile Hf isotopic signature for a group of truly high-silica igneous rocks (Ewart et al., 1992; Bryan et al., 2000).

We highlight through this work the potential bias of using isotopic characteristics of a single igneous/tectonic event or a limited duration of magmatism (<100 Myr) to characterise the age and compositional characteristics of the evolving continental crust. Isotope studies on NEO granitoids have suggested that because of their juvenile character and limited isotopic diversity, NEO granites have been derived from relatively homogenous juvenile crustal or mantle sources and built up during mid to late Paleozoic subduction (e.g., Kemp et al., 2009). The observation that most exposed rocks in the NEO are Devonian to Triassic has been used to support this (e.g., Jell, 2013; Rosenbaum, 2018). However, almost all the isotopic characterisation of the NEO presented in Kemp et al (2009) has been based only on granitic rocks from ~305-250 Ma (Belousova et al., 2006; Kemp et al., 2009), and thus the more strongly radiogenic isotopic compositions of older granites and young Tertiary igneous rocks have been missed.

Our study also has implications for how edges of cratons and Precambrian crust are defined (e.g., Tasman Line of eastern Australia, Hill, 1951; Direen & Crawford, 2003; the initial Sr isotope line of western North America, Kistler & Peterman, 1973; Armstrong et al., 1977). Our study area lies well east of interpreted positions of the Tasman Line which was thought to mark the boundary between the Tasmanides and the Precambrian craton (Direen & Crawford, 2003). Yet, Mesoproterozoic and Paleoproterozoic crustal materials were involved in the Permo-Carboniferous igneous events within our study area. Middle Triassic to Tertiary igneous events involved only Phanerozoic crustal sources and studies restricted to these intrusions would miss this Precambrian crustal contribution to granitic magmatism. Additionally, the occurrence of Precambrian zircon inheritance in granulite xenoliths of

Miocene mafic rocks (Allen & Williams, 1998), in Cretaceous igneous rocks (Bryan et al., 2012), and in Carboniferous igneous rocks (Table 2, Bryan et al., 2004) supports the presence of Precambrian crust east of the Tasman line.

The more extensive database for the entirety of the Tasmanides (Fig. 9), now available a decade after the work by Kemp et al. (2009), shows the zircon ages and associated Hf isotope composition of the three granite types, including samples from the Macquarie arc (I-type) since the Cambrian. The compilation includes recent work from the sparsely exposed Thomson Orogen (Cross et al., 2018; Siegel et al., 2018; Waltenberg et al., 2018) and granites analysed from northern Queensland (Murgulov et al., 2008; Murgulov et al., 2013). These data show that the main trend toward a more juvenile character holds from ~450 Ma into the Mesozoic, but for example, while the Macquarie arc was active in the Ordovician, strongly crustal I- and S-type granites were being emplaced in the Lachlan, and A-type granites of more intermediate isotopic character in the Delamerian orogen (Fig. 9b). Of note is that the Tertiary rocks in our study area have neutral to positive Hf isotope values like the A-types of the Delamerian, some 450 Myr older. When the data are partitioned at the regional scale, Figs 9c-h show that no obvious systematic granite type progressions exist in terms of either isotopic composition or chemical affinity (I-, S- or A-type). In summary, to fully unravel the evolution of continental-scale tectonomagmatic systems, complementary regional and local-scale approaches and long-term perspectives are required.

CONCLUSIONS

This study has taken a small spatial, but long-term temporal scale examination of igneous rocks to better understand crustal evolution and the impacts of past igneous events on crustal differentiation and the composition of successive crust-derived magmas. A number of key conclusions arise from our integrated mineralogic, whole-rock geochemical, zircon

chronochemical and Hf isotopic study:

1. Petrographic and whole-rock chemical characteristics of silicic igneous rocks define two major compositional groups that were produced over a ~350 Myr period: Group 1 comprises voluminous Permo-Carboniferous and Early Cretaceous I-type igneous rocks, and Group 2 includes less voluminous Middle Triassic, Middle Cretaceous and Tertiary A-type igneous rocks. Over time, generation and emplacement of these compositional groups alternated.

2. Heat production values, used as a monitor of crustal differentiation, show a "zig-zag" pattern with time. Early Carboniferous, Middle Cretaceous and Tertiary igneous rocks exhibit the highest heat production values (up to 3.8 $\mu W/m^3$). These temporal heat production variations, coupled with mineralogical and compositional differences do not correlate with fractional crystallisation indices, but are dominantly source controlled. This is strongly indicated by the correlation between heat production values of the igneous rocks and zircon Hf isotopic composition. The two mineralogical and compositional groups are interpreted to be derived from at least two different bulk crustal sources: 1) Group 1 is from a crustal source with an overall amphibolitic metaigneous composition and which had a significant contribution of mantle-derived magmas intruded into the lower to middle crust during previous tectonomagmatic events, and 2) Group 2 is from a magnesian tonalitic to granodioritic source composition more likely located in the middle to upper crust. We infer that these source types have been repeatedly tapped over a period of 350 Myr.

3. By combining Hf model ages, zircon inheritance, geochemical information (HPE and silica contents), surface exposure, and constraints from the regional geology, we propose that the compositional groups arise from two end-member types of igneous

systems: 1) large-scale magmatic systems that are more energetic, being driven by higher rates and larger volumes of basaltic underplating and intrusion (i.e. basification), promote extensive crustal melting of multiple crustal sources to produce large volumes of I-type igneous rocks with whole-rock compositions that trend towards bulk crustal compositions (Group 1 igneous rocks); versus 2) small-scale systems that cause more localised crustal melting of more limited source compositions (Table 5; Fig. 7) producing lesser volumes of A-type igneous rocks (Group 2). Crustal sources for Group 2 igneous rocks are inferred to be the products of previous crustal partial melting events explaining the A-type chemical affinities and more elevated heat production values.

4. A close correspondence is observed between heat production and zircon Hf isotopic compositions. Rocks with elevated heat production values exhibit more unradiogenic (crustal) isotopic signatures indicating a significant involvement of Precambrian material in the magma source regions. Precambrian igneous rocks in Australia are known to be more high heat-producing in comparison to other continents (Sandiford et al., 2001; McLaren & Powell, 2014), helping explain the relatively higher heat production values of granitic rocks derived from such a source.

5. Zircon Hf isotopes are thought to record a long-term trend towards more isotopically juvenile compositions over time. This had been observed by Allen et al. (1997) and Allen (2000) in the study area based on whole-rock Nd and Sr isotopic compositions, and at orogen-scales by Kemp et al. (2009), Collins et al. (2011), and Nelson & Cottle (2018). The mechanisms for the observed trends are debated. The coupled temporal shift from S- to I-type granites in the NEO (Kemp et al., 2009) was not observed here at the local scale. The removal of ancient crust by mechanical subduction erosion or

thermal erosion in an arc- to back-arc setting (Collins et al., 2011), or a greater contribution of mantle-derived magmas as the tectonic setting evolves from arc to back-arc to intraplate settings do not explain the data presented here. We interpret the long-term temporal compositional trends of igneous rocks in the study area to result from the combination of several mechanisms. First, melt depletion whereby older crustal materials become more refractory. Second, the intrusion of compositionally monotonous mantle-derived magmas to the crust add to the crustal profile and can result in significant "crustal jacking" of older crustal materials from the lower crust to higher crustal positions. In large-scale magmatic systems, large fluxes into the lower crust can result in extensive crustal melting of multiple crustal sources, leading to blended and more uniform isotopic signatures. In contrast, small-scale magmatic systems are more localised, and may partially melt crustal materials located at higher crustal levels or the products of previous partial melting events, inheriting their isotopic characteristics, and thereby reversing apparent long-term trends to more positive Hf isotopic signatures. We find that zircon Hf isotopic composition and evolution are less directly connected to the tectonic state at the time of magmatism (cf. Kemp et al., 2009; Nelson & Cottle, 2018).

6. We find igneous-dominated processes in extensional settings (back-arc, intraplate) can have profound effects on crustal architecture, growth, differentiation, isotopic evolution and long-term temporal-compositional trends in magmas.

7. Today's picture of the whole of the Tasmanides, from a compilation of this work and others, indicates a complicated growing continent in which unidirectional trends in granite type over time are not necessarily the norm. A trend to an overall more juvenile isotopic character can be present but local and regional excursions, and long-

term (>100 Myr) deviations to this trend exist.

Our findings highlight the importance of integrating whole-rock geochemical data and isotopic information with a holistic understanding of the region's geological history to develop a picture of long-term igneous trends from which the most-informed interpretations on mantle contributions and crustal evolution can be made.

ACKNOWLEDGEMENTS

The authors thank A. Greig for whole-rock trace element compositions, S. Eggins for setting up the MC-ICP-MS for Hf analyses on zircon, and B. Bultitude for field-work assistance. CS acknowledges financial support from QUT Postgraduate Research Award and Queensland Geothermal Energy Centre of Excellence at the University of Queensland. CA thanks Bruce Chappell for introducing her to the region 29 years ago. We thank an anonymous reviewer, Mihai Ducea and Anthony Kemp for their thorough reviews that helped improved this manuscript, as well as Simon Turner, Marjorie Wilson and Gerhard Worner for editorial support.

CAPTIONS

FIGURES

Fig. 1. Map of the Tasmanides providing the regional tectonic framework and illustrating the location of the study area. Extents of the tectonic elements are from Glen (2005), (Purdy et al., 2013) and Fergusson & Henderson (2015). The Tasman line is from Veevers & Powell (1984) **165 mm**

Fig. 2. Geological map of the study area showing intrusive and extrusive rocks for all outcropping igneous events. Local towns (e.g. Bowen, Mackay and Collinsville) are indicated by boxed text. Geological provinces are also indicated in italics (e.g. Whitsundays Province) and are separated from each other by bold dashed lines. NEO, New England Orogen. Modified after Allen et al. (1997, 1998), Bryan et al. (2004), Parianos (1993), 1:250000 geological maps of Bowen, Ayr, Proserpine, Mackay, Mount Coolon, Carmila and Mirani (Jensen et al., 1966; Paine et al., 1968; Clarke et al., 1971; Gregory et al., 1971; Hutton et al., 1997; Bultitude & Roberts, 2004; Jensen et al., 2004), the 1:2000000 geological map of Queensland (Geological Survey of Queensland, 2012), and the million scale geological map of Australia (Raymond et al., 2012). **165 mm**

Fig. 3. Rock classification schemes illustrating the compositional variability of the igneous rocks from the study area. **(a)** TAS diagram after LeBas et al. (1986); **(b)** Ferroan vs Magnesian classification after Frost et al. (2001); **(c)** Modified Alkali-Lime Index (MALI) vs SiO_2 content; a is alkalic, a-c is alkali-calcic, c-a is calc-alkalic and c is calcic; after Frost et al. (2001); all silica contents plotted; **(d)** Shand's index after Maniar and Piccoli (1989); only igneous rocks with SiO_2 >70 wt% plotted; **(e)** Discrimination between I- and S-types and A-type; after Whalen et al. (1987); only SiO_2 >70 wt% plotted. (a) to (e): N=76 samples; **(f)** Average of high-silica igneous rocks (SiO_2 >70 wt%) for all igneous events normalised to the bulk crustal values of Rudnick & Gao (2003). Outliers were not considered for the average. **165 mm**

Fig. 4. (a) Heat Production over time for high-silica igneous rocks (>70 wt% SiO_2) with associated tectonic settings. The grey bar indicates the timing of the Hunter Bowen Orogeny (HBO). Legend is as per Fig. 3; **(b)** Heat production spectrum over time for igneous rocks with SiO_2 > 70 wt%, colour coded for different Rb/Sr ratios, data are from this study. **80mm**

Fig. 5. Isotopic evolution plots. **(a)** ƐHf versus time; crustal evolution curves are drawn using a Lu/Hf equal to 0.0125 after Chauvel et al. (2014); $^{176}Hf/^{177}Hf$ is calculated using a decay constant $\lambda^{176}Lu=1.867.10^{-11}$ y^{-1} (Söderlund et al., 2004), ƐHf is calculated using chondritic values from Bouvier et al. (2008); CHUR is Chondritic Uniform Reservoir. The depleted mantle line is drawn using values from Griffin et al. (2000); **(b)** ƐNd versus time and **(c)** Sr isotopic ratios versus time.; Note the similarity in zircon Hf and whole-rock ƐNd values over time. Data are from Ewart et al. (1992), Parianos (1993), Allen et al. (1997), Allen (2000), Allen (unpublished data) and Champion et al. (2013). **165 mm**

Fig. 6. Schematic crustal evolution diagram for the Bowen-Mackay area. **(a)** Tectonic settings and temporal variations in heat production; **(b)** zircon Hf isotopic compositions (ƐHf). 1 represents samples CAP-04 & CUR-02, 2 VIO-01, 3 MH-01 and 4 BN-02 & HECT-01. 1 & 2 are more heat-producing and more unradiogenic while 3 & 4 are less heat-producing and more radiogenic. Note the mirror pattern between Hf and heat production

values (all except Middle Triassic). Group 1 are shown in blues and Group 2 in red, orange and yellow. **165 mm**

Fig. 7. Comparison of partial melting experiment compositions with igneous compositions from the study area (Siegel, 2015). From top to bottom, Fe-index, MALI and K_2O versus SiO_2 for I-type Group 1 igneous rocks (left) and A-type Group 2 igneous rocks (right) displaying the kernel density estimates from compiled geochemical data from Siegel (2015). Shown for comparison are relevant partial melting experiments from the literature. Abbreviations are: s.m: starting material; e.m.: experimental melt; P & B 1995 are data from Patiño Douce & Beard (1995), B & L 1991 from Beard & Lofgren (1991), J & K 2001 from Johannes & Koepke (2001), PD 1997 from Patiño Douce (1997) Patino Douce (1997) and S & J 1992 from Skjerlie & Johnston (1992). **165 mm**

Fig. 8. Schematic crustal evolution model for the Bowen-Mackay area. **(a)** Pie charts show proportion of crustal sources and surface area of exposed igneous rocks (pies size). Low HP and High HP refer to samples that have higher heat-production (1: CAP-04 & CUR-02, 2: VIO-01) and lower heat production (3: MH-01, 4: BN-02 & HECT-01), respectively. Note the crustal sources for high HP samples include a greater proportion of Precambrian materials in comparison to low HP samples. **(b)** Schematic crustal profiles over time (not at scale; crustal thinning and exhumation not considered). The pre-existing crustal profile (prior magmatism) is shown in dull shade. For example, the crustal profile in the Late Carboniferous comprises the Early Carboniferous profile in dull shade, with the addition of new mantle-derived basaltic underplate at the bottom and products of the partial melting event at the top. The black outline rectangles indicate the zone of crust that is partially melted and reworked in each tectonomagmatic event. Group 1 igneous rocks are sourced from the lower to middle crust, while the Group 2 igneous rocks are sourced from the mid to upper crust. Note that Middle Cretaceous magmatism is combined with the Early Cretaceous event in this figure due to the lack of Hf isotope data for the Middle Cretaceous. A and B both show the increasing proportion of younger crustal sources over time essentially due to the accumulation of mantle-derived basaltic underplate, also known as “basification”, during those successive igneous events. **165 mm**

Fig. 9. Zircon Hf isotopic evolution curves for different orogens in Eastern Australia. **(a)** Tasmanides evolution from Kemp et al., (2009); **B.** ƐHf vs age for the Tasmanides based on the expanded dataset; **(c), (d), (e), (f), (g) and (h)** ƐHf vs age for the Delamerian, Lachlan, Thomson orogens, North Queensland, northern NEO, and southern NEO, respectively; symbol legend shown in B. Data for B to H are from this study, and published data (Kemp et al., 2005; Belousova et al., 2006; Kemp et al., 2007; Murgulov et al., 2008; Fu et al., 2009; Kemp et al., 2009; Glen et al., 2011; Phillips et al., 2011; Shaw et al., 2011; Murgulov et al., 2013; Cross et al., 2018; Siégel et al., 2018b; Waltenberg et al., 2018). Crustal evolution curves are drawn using a Lu/Hf equal to 0.0125 after Chauvel et al. (2014); $^{176}Hf/^{177}Hf$ is calculated using a decay constant $\lambda^{176}Lu=1.867.10^{-11}$ y^{-1} (Söderlund et al., 2004), ƐHf is calculated using chondritic values from Bouvier et al. (2008); CHUR is Chondritic Uniform Reservoir. The depleted mantle line is drawn using values from Griffin et al. (2000). **165 mm**

Fig. 10. Conceptual model illustrating the switching of large-scale (Group 1) and small-scale (Group 2) magmatic systems and its consequences on crustal evolution and heat-production over time. The Phanerozoic crust underlying the Precambrian crust after T_1 results from the addition of Phanerozoic mantle-derived basaltic underplates. Note that for Group 1 igneous rocks, new silicic magmas can derive from partial melting of the heated crust overlying new

mantle-derived basaltic underplates (T_1), and may result from partial remelting of previous mantle-derived basaltic underplates (T_2). For Group 2 igneous rocks, rising of mantle-derived magmas at high levels in the crustal profile cause partial remelting of tonalite/granodiorites formed during previous tectonomagmatic events (T_3). The heat production character of igneous rocks is dominantly controlled by the nature of crustal sources; Magmas generated at T_1 and T_3, have elevated heat-production values as their sources are enriched in HPE: a Precambrian crust, and a tonalite/granodiorite source, respectively. In contrast, magmas generated at T_2 are less heat-producing due to crustal melting of HPE-poor Phanerozoic crust added at T_1. **165 mm**

TABLES

Table 1. List of Phanerozoic events in Queensland.
Table 2. LA-ICP-MS U-Pb zircon age summary; Weighted mean ages (uncertainties are 2σ and internal/external). Ages below 1000 Ma are $^{206}Pb/^{238}U$ ages, and ages above 1000 Ma are $^{207}Pb/^{206}Pb$ ages.
Table 3. Summary of mineralogical and compositional characteristics focussing on high-silica igneous rocks from all tectonomagmatic events in the Bowen-Mackay area.
Table 4. Scale of magmatism for Group 1 and Group 2 igneous rocks
Table 5. Nature of igneous crustal sources. In bold are dominant crustal sources as illustrated in the pies of Fig. 8.

APPENDICES

Appendix 1. Animated gif illustrating long-lived igneous activity in the study area. Note that Early Cretaceous are blanketed by Middle Cretaceous extrusive rocks.
Appendix 2. Results - Major and trace element data; all analyses are normalised to 100% on anhydrous basis.
Appendix 3. Zircon chronochemistry and Hf isotope in zircon
Appendix 4. Analytical methods; **A.** sample preparation and analytical technique for whole-rock chemistry; **B.** Sample preparation and analytical techniques for zircon U-Pb dating by LA-ICP-MS and Hf isotopes in zircons
Appendix 5. Supplementary figure: Representative CL images for zircon grains from Bowen-Mackay igneous rocks: **(a)** Early Carboniferous Cape Upstart granodiorite (CAP-04), **(b)** Early Carboniferous Mount Curlewis syenogranite (CUR-02), **(c)** Late Carboniferous Viola Creek monzogranite (VIO-01), **(d)** Permian Grant Creek monzogranite (GRA-01), **(e)** Middle Triassic Shaw Island alkali-feldspar granite (SH47), **(f)** Middle Triassic Passage Islet granodiorite (GLO-02), **(g)** Early Cretaceous Roundback granodiorite, **(h)** & **(i)** Early Cretaceous Highlander Bonnet granodiorite to monzogranite, **(j)** Tertiary Belmunda obsidian, and **(k)** Tertiary Mount Blackwood granodiorite. Circles indicate the location of analyses. Scale is the same for all images.
Appendix 6. Zircon chemistry for all samples from the Bowen-Mackay region. Analyses affected by inclusions are excluded. **(a)** Dy_N/Lu_N versus Th/U. N indicates concentrations were normalised to chondrite using values from Sun and McDonough (1989). (**b)** Log(U) versus Zr/Hf.
Appendix 7. Geophysical evidence for mafic underplating. Both figures illustrate, along the coast of Queensland (including the study area), elevated seimic velocities: 1) at the base of the crust and 2) within the bottom crustal layer and upper mantle, providing strong evidence for mafic underplating in this area. These maps were created using AuSeis data from Qashqai et al (2019) and empirical bayesian kriging interpolation from the geostatistical analytist toobox from ArcGIS. The output cell size is 0.5.

T. Qashqai, M., Saygin, E., and Kennett, B.L.N. (2019), Crustal Imaging with Bayesian Inversion of Teleseismic P_wave Coda Autocorrelation, J. Geophys. Res. Solid Earth, 124, https://doi.org/10.1029/2018JB017055

REFERENCES

Allen CM (2000) Evolution of a post-batholith dike swarm in central coastal Queensland, Australia: arc-front to backarc? *Lithos,* 51 (4): 331-349.

Allen CM & Williams IS (1998) *Crustal ages determined by SHRIMP dating of zircon from granulite xenoliths, New England Orogen, central coastal Queensland*. Abstracts - Geological Society of Australia. Geological Society of Australia, Sydney, N.S.W., Australia, 8 p.

Allen CM, Williams IS, Stephens CJ & Fielding CR (1998) Granite genesis and basin formation in an extensional setting: the magmatic history of the northernmost New England Orogen. *Australian Journal of Earth Sciences,* 45 (6): 875-888.

Allen CM, Wooden JL & Chappell BW (1997) Late Paleozoic crustal history of central coastal Queensland interpreted from geochemistry of Mesozoic plutons: The effects of continental rifting. *Lithos,* 42 (1-2): 67-88.

Anderson S (2016) *Probing the crust: Time, Space & Source relationships of granitoids at Cape Upstart, Northeast QLD.* Queensland University of Technology. Honours Thesis (unpublished) 67 p.

Annen C, Blundy JD & Sparks RSJ (2006) The Genesis of Intermediate and Silicic Magmas in Deep Crustal Hot Zones. *Journal of Petrology,* 47 (3): 505-539.

Armstrong RL, Taubeneck WH & Hales PO (1977) Rb-Sr and K-Ar geochronometry of Mesozoic granitic rocks and their Sr isotopic composition, Oregon, Washington, and Idaho. *Geological Society of America Bulletin,* 88 (3): 397-411.

Artemieva IM, Thybo H, Jakobsen K, Sørensen NK & Nielsen LS (2017) Heat production in granitic rocks: Global analysis based on a new data compilation GRANITE2017. *Earth-Science Reviews,* 172: 1-26.

Bain JHC & Draper JJ (1997) *North Queensland Geology,* Australian Geological Survey Organization/Queensland Department of Mines and Energy. 600 p.

Beard JS & Lofgren GE (1991) Dehydration Melting and Water-Saturated Melting of Basaltic and Andesitic Greenstones and Amphibolites at 1, 3, and 6. 9 kb. *Journal of Petrology,* 32 (2): 365-401.

Belousova EA, Griffin WL & O'Reilly SY (2006) Zircon Crystal Morphology, Trace Element Signatures and Hf Isotope Composition as a Tool for Petrogenetic Modelling: Examples From Eastern Australian Granitoids. *Journal of Petrology,* 47 (2): 329-353.

Belousova EA, Kostitsyn YA, Griffin WL, Begg GC, O'Reilly SY & Pearson NJ (2010) The growth of the continental crust: Constraints from zircon Hf-isotope data. *Lithos,* 119 (3–4): 457-466.

Blichert-Toft J & Albarède F (1997) The Lu-Hf isotope geochemistry of chondrites and the evolution of the mantle-crust system. *Earth and Planetary Science Letters,* 148 (1–2): 243-258.

Bonin B (2007) A-type granites and related rocks: Evolution of a concept, problems and prospects. *Lithos,* 97 (1-2): 1-29.

Bouvier A, Vervoort JD & Patchett PJ (2008) The Lu–Hf and Sm–Nd isotopic composition of CHUR: Constraints from unequilibrated chondrites and implications for the bulk composition of terrestrial planets. *Earth and Planetary Science Letters,* 273 (1–2): 48-57.

Bruce MC & Niu Y (2000) Evidence for Palaeozoic magmatism recorded in the Late Neoproterozoic Marlborough ophiolite, New England Fold Belt, central Queensland. *Australian Journal of Earth Sciences,* 47 (6): 1065-1076.

Bruce MC, Niu Y, Harbort T & Holcombe R (2000) Petrological, geochemical and geochronological evidence for a Neoproterozoic ocean basin recorded in the Marlborough terrane of the northern New England Fold Belt. *Australian Journal of Earth Sciences,* 47 (6): 1053-1064.

Bryan SE, Allen CM, Holcombe RJ & Fielding CR (2004) U-Pb zircon geochronology of Late Devonian to Early Carboniferous extension-related silicic volcanism in the northern New England Fold Belt. *Australian Journal of Earth Sciences,* 51 (5): 645-664.

Bryan SE, Constantine AE, Stephens CJ, Ewart A, Schön RW & Parianos J (1997) Early Cretaceous volcano-sedimentary successions along the eastern Australian continental margin: implications for the break-up of eastern Gondwana. *Earth and Planetary Science Letters,* 153 (1): 85-102.

Bryan SE, Cook A, Allen CM, Siegel C, Purdy D, Greentree J & Uysal T (2012) Early-mid Cretaceous tectonic evolution of eastern Gondwana: From silicic LIP magmatism to continental rupture. *Episodes,* 35 (1): 142-152.

Bryan SE, Ewart A, Stephens CJ, Parianos J & Downes PJ (2000) The Whitsunday Volcanic Province, Central Queensland, Australia: lithological and stratigraphic investigations of a silicic-dominated large igneous province. *Journal of Volcanology and Geothermal Research,* 99 (1-4): 55-78.

Bryan SE, Holcombe RJ & Fielding CR (2001) Yarrol terrane of the northern New England Fold Belt: forearc or backarc? *Australian Journal of Earth Sciences,* 48 (2): 293-316.

Bryan SE, Holcombe RJ, Fielding CR & Cook A (2003) Stratigraphy, facies architecture and tectonic implications of the Upper Devonian to Lower Carboniferous Campwyn Volcanics of the northern New England Fold Belt - Reply. *Australian Journal of Earth Sciences,* 51 (3): 453-458.

Bryan SE, Siegel C, Allen CM, Gust D, Purdy DJ & Martin J (2015) *Field Guide to Granite Bay, Noosa Heads,* Geological Society of Australia.

Bultitude RJ & Roberts CW (2004) *Carmila sheet 8754 first edition 2004*. Department of Natural Resources, Mines and Energy. Map

Cawood PA (1984) The development of the SW Pacific margin of Gondwana; correlations between the Rangitata and New England orogens. *Tectonics,* 3: 539-553.

Cawood PA, Hawkesworth CJ & Dhuime B (2013) The continental record and the generation of continental crust. *Geological Society of America Bulletin,* 125 (1-2): 14-32.

Champion DC (2013) *Neodymium depleted mantle model age map of Australia: explanatory notes and user guide.* Geoscience Australia. Record 2013/44, 209 p.

Chappell BW & White AJR (1974) Two contrasting granite types. *Pacific Geology,* 8: 173-174.

Chappell BW & White AJR (2001) Two contrasting granite types: 25 years later. *Australian Journal of Earth Sciences,* 48 (4): 489-499.

Chauvel C, Garçon M, Bureau S, Besnault A, Jahn BM & Ding Z (2014) Constraints from loess on the Hf-Nd isotopic composition of the upper continental crust. *Earth and Planetary Science Letters,* 388: 48-58.

Clarke DE, Paine AGL, Jensen AR & Brown PJ (1971) *Proserpine Sheet SF55-04 and 1:250,000 Geological series - Explanatory notes*. Map

Clemens JD (2003) S-type granitic magmas-petrogenetic issues, models and evidence. *Earth Science Reviews,* 61 (1-2): 1-18.

Clemens JD, Holloway JR & White AJR (1986) Origin of an A-type granite; experimental constraints. *American Mineralogist,* 71 (3-4): 317-324.

Clemens JD, Stevens G & Bryan SE (2020) Conditions during the formation of granitic magmas by crustal melting – Hot or cold; drenched, damp or dry? *Earth-Science Reviews*, 200: 102982.
Collins CDN (1988) *Seismic velocities in the crust and upper mantle of Australia.* Bureau of Mineral Resources, Geology and Geophysics.
Collins W (1991) A reassessment of the 'Hunter-Bowen Orogeny': Tectonic implications for the southern New England fold belt. *Australian Journal of Earth Sciences,* 38 (4): 409-423.
Collins WJ, Belousova EA, Kemp AIS & Murphy JB (2011) Two contrasting Phanerozoic orogenic systems revealed by hafnium isotope data. *Nature Geosci,* 4 (5): 333-337.
Collins WJ, Huang H-Q & Jiang X (2016) Water-fluxed crustal melting produces Cordilleran batholiths. *Geology,* 44 (2): 143-146.
Collins WJ, Murphy JB, Johnson TE & Huang H-Q (2020) Critical role of water in the formation of continental crust. *Nature Geoscience*: 1-8.
Condie KC, Arndt N, Davaille A & Puetz SJ (2017) Zircon age peaks: Production or preservation of continental crust? *Geosphere,* 13 (2): 227-234.
Condie KC, Bickford ME, Aster RC, Belousova E & Scholl DW (2011) Episodic zircon ages, Hf isotopic composition, and the preservation rate of continental crust. *GSA Bulletin,* 123 (5-6): 951-957.
Condie KC, Puetz SJ & Davaille A (2018) Episodic crustal production before 2.7 Ga. *Precambrian Research,* 312: 16-22.
Cook AG, Bryan SE & Draper JJ (2013) Post-orogenic Mesozoic basins and magmatism. *In:* Jell P (ed.) *Geology of Queensland.* Brisbane, QLD: Geological Survey of Queensland pp. 515-576.
Creaser RA, Price RC & Wormald RJ (1991) A-type granites revisited: Assessment of a residual-source model. *Geology,* 19 (2): 163-166.
Cross AJ, Purdy DJ, Champion DC, Brown DD, Siégel C & Armstrong RA (2018) Insights into the evolution of the Thomson Orogen from geochronology, geochemistry and zircon isotopic studies of magmatic rocks. *Australian Journal of Earth Sciences,* in press.
Dewey JF & Windley BF (1981) Growth and differentiation of the continental crust. *Philosophical Transactions of the Royal Society of London. Series A, Mathematical and Physical Sciences,* 301 (1461): 189-206.
Dhuime B, Hawkesworth C & Cawood P (2011) When continents formed. *Science,* 331 (6014): 154-155.
Direen NG & Crawford AJ (2003) The Tasman Line: Where is it, what is it, and is it Australia's Rodinian breakup boundary? *Australian Journal of Earth Sciences,* 50 (4): 491-502.
Eby GN (1992) Chemical subdivision of the A-type granitoids; petrogenetic and tectonic implications. *Geology,* 20 (7): 641-644.
Ewart A, Schon RW & Chappell BW (1992) The Cretaceous volcanic-plutonic province of the central Queensland (Australia) coast - a rift related "calc-alkaline' province. *Transactions - Royal Society of Edinburgh: Earth Sciences,* 83 (1-2): 327-345.
Fergusson CL & Henderson RA (2015) Early Palaeozoic continental growth in the Tasmanides of northeast Gondwana and its implications for Rodinia assembly and rifting. *Gondwana Research,* 28 (3): 933-953.
Förster H-J, Tischendorf G, Trumbull RB & Gottesmann B (1999) Late-Collisional Granites in the Variscan Erzgebirge, Germany. *Journal of Petrology,* 40 (11): 1613-1645.
Frost BR, Barnes CG, Collins WJ, Arculus RJ, Ellis DJ & Frost CD (2001) A Geochemical Classification for Granitic Rocks. *Journal of Petrology,* 42 (11): 2033-2048.

Fu B, Mernagh TP, Kita NT, Kemp AIS & Valley JW (2009) Distinguishing magmatic zircon from hydrothermal zircon: A case study from the Gidginbung high-sulphidation Au–Ag–(Cu) deposit, SE Australia. *Chemical Geology,* 259 (3–4): 131-142.

Glen RA (2005) The Tasmanides of eastern Australia. *Geological Society, London, Special Publications,* 246 (1): 23-96.

Glen RA, Saeed A, Quinn CD & Griffin WL (2011) U–Pb and Hf isotope data from zircons in the Macquarie Arc, Lachlan Orogen: Implications for arc evolution and Ordovician palaeogeography along part of the east Gondwana margin. *Gondwana Research,* 19 (3): 670-685.

Green TH (1969) High-pressure experimental studies on the origin of anorthosite. *Canadian Journal of Earth Sciences,* 6 (3): 427-440.

Gregory CM, Malone EJ, Jensen AR, Paine AGL, Olgers F, Clarke DE, Forbes VR, Webb EA & Crapp CE (1971) *Bowen Sheet SF55-03 and 1:250,000 Geological series - Explanatory notes*. Map

Griffin WL, Pearson NJ, Belousova E, Jackson SE, van Achterbergh E, O'Reilly SY & Shee SR (2000) The Hf isotope composition of cratonic mantle: LAM-MC-ICPMS analysis of zircon megacrysts in kimberlites. *Geochimica et Cosmochimica Acta,* 64 (1): 133-147.

Griffin WL, Sutherland FL & Hollis JD (1987) Geothermal profile and crust-mantle transition beneath east-central Queensland: Volcanology, xenolith petrology and seismic data. *Journal of Volcanology and Geothermal Research,* 31 (3–4): 177-203.

Harley SL & Kelly NM (2007) Zircon Tiny but Timely. *Elements,* 3 (1): 13-18.

Hawkesworth CJ, Cawood P & Dhuime B (2013) Continental growth and the crustal record. *Tectonophysics,* 609 (0): 651-660.

Hawkesworth CJ, Cawood PA & Dhuime B (2016) Tectonics and crustal evolution. *GSA Today*.

Hill D (1951) Geology. *In:* Mack G (ed.) *Handbook of Queensland.* Australian Association for the Advancement of Science, Brisbane. pp. 13-24.

Holcombe RJ, Stephens CJ, Fielding CR, Gust D, Little TA, Sliwa R, Kassan J, McPhie J & Ewart A (1997) Tectonic evolution of the northern New England Fold Belt: the Permian–Triassic Hunter–Bowen event. *In:* Ashley PM & Flood PG (eds.) *Tectonics and metallogenesis of the New England Orogen: Alan H. Voisey Memorial Volume.* Geological Society of Australia, Special Publication 19 pp. 52–65.

Hunter R & Sparks R (1987) The differentiation of the Skaergaard intrusion. *Contributions to Mineralogy and Petrology,* 95 (4): 451-461.

Huppert HE & Sparks J (1988) The generation of granitic magmas by intrusion of basalt into continental crust. *J. Petrology,* 29 (3): 599-624.

Huppert HE, Stephen R & Sparks J (1985) Cooling and contamination of mafic and ultramafic magmas during ascent through continental crust. *Earth and Planetary Science Letters,* 74 (4): 371-386.

Hutton LJ (2004) *Petrogenesis of I- and S-type Granites in the Cape River - Lolworth area, northeastern Queensland - Their contribution to an understanding of the Early Palaeozoic Geological History of northeastern Queensland.* Queensland University of Technology. PhD Thesis (unpublished) 216 p.

Hutton LJ, Law SR, Grimes KG, Belcher RL & McLennan TP (1997) *Mount Coolon, Sheet SF55-07 Second Edition 1997 and 1:250,000 Geological series - Explanatory notes*. Map

Hyndman RD, Currie CA & Mazzotti SP (2005) Subduction zone backarcs, mobile belts, and orogenic heat. *GSA Today,* 15 (2): 4-10.

Iizuka T, Campbell IH, Allen CM, Gill JB, Maruyama S & Makoka F (2013) Evolution of the African continental crust as recorded by U–Pb, Lu–Hf and O isotopes in detrital zircons from modern rivers. *Geochimica et Cosmochimica Acta,* 107: 96-120.

Irvine T & Baragar W (1971) A guide to the chemical classification of the common volcanic rocks. *Canadian Journal of Earth Sciences,* 8 (5): 523-548.

Isern AR, Anselmetti FS, Blum P & al. e (2002) *Leg 194 of the cruises of the Drilling Vessel JOIDES Resolution Townsville, Australia, to Apra Harbor, Guam, Sites 1192-1199, 3 January - 2 March 2001*. Initial Reports, Proceedings of the Ocean Drilling Program, Initial Reports. 194.

Jagoutz O & Klein B (2018) On the importance of crystallization-differentiation for the generation of SiO2-rich melts and the compositional build-up of arc (and continental) crust. *American Journal of Science,* 318 (1): 29-63.

Jell PA (2013) *Geology of Queensland,* Brisbane, Queensland, Geological Survey of Queensland. 928 p.

Jensen AR, Gregory CM, Forbes VR, White WC & Brown GA (1966) *Mackay Sheet SF55-08 and 1:250,000 Geological Series - Explanatory notes*. Map

Jensen AR, Gregory CM, Forbes VR, White WC, Brown GA, Willmott WW, Martin JE, Von Gnielinski FE, Bultitude RJ, Withnall IW & Hutton LJ (2004) *Mirani, Sheet 8655, First edition 2004*. Map

Johannes W & Holtz F (1996) *Petrogenesis and experimental petrology of granitic rocks,* New York, Springer.

Johannes W & Koepke J (2001) Incomplete reaction of plagioclase in experimental dehydration melting of amphibolite. *Australian Journal of Earth Sciences,* 48 (4): 581-590.

Johnson RW, Knutson J & Taylor SR (1989) *Intraplate volcanism: in eastern Australia and New Zealand*, Cambridge University Press. 444 p.

Kemp AIS & Hawkesworth CJ (2014) 4.11 - Growth and Differentiation of the Continental Crust from Isotope Studies of Accessory Minerals. *In:* Holland HD & Turekian KK (eds.) *Treatise on Geochemistry (Second Edition).* Oxford: Elsevier pp. 379-421.

Kemp AIS, Hawkesworth CJ, Collins WJ, Gray CM & Blevin PL (2009) Isotopic evidence for rapid continental growth in an extensional accretionary orogen: The Tasmanides, eastern Australia. *Earth and Planetary Science Letters,* 284 (3-4): 455-466.

Kemp AIS, Hawkesworth CJ, Foster GL, Paterson BA, Woodhead JD, Hergt JM, Gray CM & Whitehouse MJ (2007) Magmatic and crustal differentiation history of granitic rocks from Hf-O isotopes in zircon. *Science,* 315 (5814): 980-983.

Kemp AIS, Wormald RJ, Whitehouse MJ & Price RC (2005) Hf isotopes in zircon reveal contrasting sources and crystallization histories for alkaline to peralkaline granites of Temora, southeastern Australia. *Geology,* 33 (10): 797-800.

Kendall BM (1992) *Geology and geochemistry of the Mt. Bauple and Mt. Kanigan area, Maryborough basin, South-east Queensland.* University of Queensland. B.Sc. Honours Thesis (unpublished) 79 p.

Kennett BL, Fichtner A, Fishwick S & Yoshizawa K (2012) Australian seismological reference model (AuSREM): mantle component. *Geophysical Journal International,* 192 (2): 871-887.

Kistler RW & Peterman ZE (1973) Variations in Sr, Rb, K, Na, and initial Sr^{87}/Sr^{86} in Mesozoic granitic rocks and intruded wall rocks in central California. *Geological Society of America Bulletin,* 84 (11): 3489-3512.

Korsch RJ, Wake-Dyster KD & Johnstone DW (1992) Seismic imaging of Late Palaeozoic—Early Mesozoic extensional and contractional structures in the Bowen and Surat basins, eastern Australia. *Tectonophysics,* 215 (3): 273-294.

Le Bas M, Le Maitre R, Streckeisen A & Zanettin B (1986) A chemical classification of volcanic rocks based on the total alkali-silica diagram. *Journal of Petrology,* 27 (3): 745-750.
Liu M & Furlong KP (1994) Intrusion and underplating of mafic magmas: thermal-rheological effects and implications for Tertiary tectonomagmatism in the North American Cordillera. *Tectonophysics,* 237 (3): 175-187.
Loiselle MC & Wones DR (1979) *Characteristics and origin of anorogenic granites*. Geological Society of America. Abstracts 11, p. 468.
Maniar PD & Piccoli PM (1989) Tectonic discrimination of granitoids. *Geological Society of America Bulletin,* 101 (5): 635-643.
Martin RF (2006) A-type granites of crustal origin ultimately result from open-system fenitization-type reactions in an extensional environment. *Lithos,* 91 (1–4): 125-136.
McCulloch MT & Gamble JA (1991) Geochemical and geodynamical constraints on subduction zone magmatism. *Earth and Planetary Science Letters,* 102 (3–4): 358-374.
McCulloch MT, Kyser TK, Woodhead JD & Kinsley L (1994) Pb-Sr-Nd-O isotopic constraints on the origin of rhyolites from the Taupo Volcanic Zone of New Zealand - Evidence for assimilation followed by fractionation from basalt. *Contributions to Mineralogy and Petrology,* 115 (3): 303-312.
McLaren S & Powell R (2014) Magmatism, orogeny and the origin of high-heat-producing granites in Australian Proterozoic terranes. *Journal of the Geological Society,* 171 (2): 149-152.
Middleton MF (1979) Heat flow in the Moomba, Big Lake and Toolachee gas fields of the Cooper Basin and implications for hydrocarbon maturation. *Exploration Geophysics,* 10: 149-155.
Murgulov V, Griffin WL & O'Reilly SY (2013) Carboniferous and Permian granites of the northern Tasman orogenic belt, Queensland, Australia: insights into petrogenesis and crustal evolution from an in situ zircon study. *International Journal of Earth Sciences,* 102 (3): 647-669.
Murgulov V, O'Reilly SY, Griffin WL & Blevin PL (2008) Magma sources and gold mineralisation in the Mount Leyshon and Tuckers Igneous Complexes, Queensland, Australia: U-Pb and Hf isotope evidence. *Lithos,* 101 (3–4): 281-307.
Paine AGL, Gregory CM, Clarke DE, Kruger NL, Tatarow A & Clarke DE (1968) *Aye Sheet SE55-15 and 1:250,000 Geological series - Explanatory notes*. Map
Parianos JM (1993) *Carboniferous to tertiary geology of the Airlie Block, northeast Queensland.* University of Queensland. M.Sc. Thesis (unpublished) 255 p.
Patchett PJ, Vervoort JD, Söderlund U & Salters VJ (2004) Lu–Hf and Sm–Nd isotopic systematics in chondrites and their constraints on the Lu–Hf properties of the Earth. *Earth and Planetary Science Letters,* 222 (1): 29-41.
Patiño Douce AE (1997) Generation of metaluminous A-type granites by low-pressure melting of calc-alkaline granitoids. *Geology,* 25 (8): 743-746.
Patiño Douce AE & Beard JS (1995) Dehydration-melting of biotite gneiss and quartz amphibolite from 3 to 15 kbar. *Journal of Petrology,* 36 (3): 707-738.
Phillips G, Landenberger B & Belousova EA (2011) Building the New England Batholith, eastern Australia—Linking granite petrogenesis with geodynamic setting using Hf isotopes in zircon. *Lithos,* 122 (1-2): 1-12.
Puetz SJ, Condie KC, Pisarevsky S, Davaille A, Schwarz CJ & Ganade CE (2017) Quantifying the evolution of the continental and oceanic crust. *Earth-Science Reviews,* 164: 63-83.

Purdy DJ (2009) *Geology of the Late Triassic Agnes Water Volcanics, central Queensland.* Brisbane. Geological Survey of Queensland. 2009/01, 46 p.

Purdy DJ, Carr PA & Brown DD (2013) *Review of the geology, mineralisation and geothermal potential of the Thomson Orogen.* Brisbane. Geological Survey of Queensland. 2013/01, 212 p.

Qashqai MT, Saygin E & Kennett BLN (2019) Crustal Imaging with Bayesian Inversion of Teleseismic P-wave Coda Autocorrelation. *Journal of Geophysical Research: Solid Earth*, 0 (ja).

Rapp RP & Watson EB (1995) Dehydration Melting of Metabasalt at 8–32 kbar: Implications for Continental Growth and Crust-Mantle Recycling. *Journal of Petrology,* 36 (4): 891-931.

Rapp RP, Watson EB & Miller CF (1991) Partial melting of amphibolite/eclogite and the origin of Archean trondhjemites and tonalites. *Precambrian Research,* 51 (1): 1-25.

Raymond OL, Liu S, Gallagher R, Highet LM & Zhang W (2012) *Surface geology of Australia, 1: 1,000,000 scale, 2012 edition*. Geoscience Australia, Canberra, Australian Capital Territory, Australia. Map

Rosenbaum G (2018) The Tasmanides: Phanerozoic Tectonic Evolution of Eastern Australia. *Annual Review of Earth and Planetary Sciences*.

Roy M, Kelley S, Pazzaglia F, Cather S & House M (2004) Middle Tertiary buoyancy modification and its relationship to rock exhumation, cooling, and subsequent extension at the eastern margin of the Colorado Plateau. *Geology,* 32 (10): 925-928.

Sandiford M, Hand M & McLaren S (2001) Tectonic feedback, intraplate orogeny and the geochemical structure of the crust: a central Australian perspective. *Special publication - Geological Society of London,* 184: 195-218.

Scherer E, Münker C & Mezger K (2001) Calibration of the Lutetium-Hafnium Clock. *Science,* 293 (5530): 683-687.

Shaw SE, Flood RH & Pearson NJ (2011) The New England Batholith of eastern Australia: Evidence of silicic magma mixing from zircon $^{176}Hf/^{177}Hf$ ratios. *Lithos,* 126 (1-2): 115-126.

Siegel C (2015) *Heat-producing element enrichment in granitic rocks, the role of crustal composition and evolution.* Queensland University of Technology. Thesis (unpublished)

Siegel C, Bryan S, Allen C, Purdy D, Cross A, Uysal I & Gust D (2018) Crustal and thermal structure of the Thomson Orogen: constraints from the geochemistry, zircon U-Pb age, and Hf and O isotopes of subsurface granitic rocks. *Australian Journal of Earth Sciences*.

Siégel C, Bryan SE, Allen CM & Gust DA (2018a) Use and abuse of zircon-based thermometers: A critical review and a recommended approach to identify antecrystic zircons. *Earth-Science Reviews,* 176: 87-116.

Siégel C, Bryan SE, Allen CM, Purdy DJ, Cross AJ, Uysal IT & Gust DA (2018b) Crustal and thermal structure of the Thomson Orogen: constraints from the geochemistry, zircon U–Pb age, and Hf and O isotopes of subsurface granitic rocks. *Australian Journal of Earth Sciences*: 1-20.

Siégel C, Bryan SE, Purdy DJ, Gust DA, Allen CM, Uysal T & Champion DC (2012) *A new database compilation of whole-rock chemical and geochronological data of igneous rocks in Queensland: a new resource for HDR geothermal resource exploration*. Proceedings of the 2011 Australian Geothermal Energy Conference, Melbourne. Geoscience Australia, pp. 239-244.

Skjerlie KP & Johnston AD (1992) Vapor-absent melting at 10 kbar of a biotite- and amphibole-bearing tonalitic gneiss: Implications for the generation of A-type granites. *Geology,* 20 (3): 263-266.

Smith R, Cameron K, McDowell F, Niemeyer S & Sampson D (1996) Generation of voluminous silicic magmas and formation of mid-Cenozoic crust beneath north-central Mexico: evidence from ignimbrites, associated lavas, deep crustal granulites, and mantle pyroxenites. *Contributions to Mineralogy and Petrology,* 123 (4): 375-389.

Söderlund U, Patchett PJ, Vervoort JD & Isachsen CE (2004) The ^{176}Lu decay constant determined by Lu–Hf and U–Pb isotope systematics of Precambrian mafic intrusions. *Earth and Planetary Science Letters,* 219 (3): 311-324.

Sparks RSJ & Marshall LA (1986) Thermal and mechanical constraints on mixing between mafic and silicic magmas. *Journal of Volcanology and Geothermal Research,* 29 (1): 99-124.

Stephens CJ (1992) *The Mungore Cauldron and Gaydah Centre: Late Triassic Large-scale Silicic Volcanism in the New England Fold Belt Near Gaydah, Southeast Queensland.* University of Queensland. PhD Thesis (unpublished) 370 p.

Stephens CJ, Schön RW, Ewart A, Flood PG & Aitchison JC (1993) *Mesozoic crustal extension in the northern New England Orogen: geochemical and isotopic evidence from large scale silicic magmatism*. New England Orogen, eastern Australia. , University of New England, Armidale. pp. 637-642.

Tatsumi Y (2005) The subduction factory: How it operates in the evolving Earth. *GSA Today,* 15 (7): 4-10.

Trail D, Bruce Watson E & Tailby ND (2012) Ce and Eu anomalies in zircon as proxies for the oxidation state of magmas. *Geochimica et Cosmochimica Acta,* 97 (0): 70-87.

Veevers JJ & Powell CM (1984) Epi-Adelaidean: regional shear. *Phanerozoic Earth History of Australia*: 278-284.

Vervoort JD & Kemp AIS (2016) Clarifying the zircon Hf isotope record of crust–mantle evolution. *Chemical Geology,* 425: 65-75.

Wainman CC, McCabe PJ & Crowley JL (2018) Solving a tuff problem: Defining a chronostratigraphic framework for Middle to Upper Jurassic nonmarine strata in eastern Australia using uranium–lead chemical abrasion–thermal ionization mass spectrometry zircon dates. *AAPG Bulletin,* 102 (6): 1141-1168.

Wainman CC, McCabe PJ, Crowley JL & Nicoll RS (2015) U–Pb zircon age of the Walloon Coal Measures in the Surat Basin, southeast Queensland: implications for paleogeography and basin subsidence. *Australian Journal of Earth Sciences,* 62 (7): 807-816.

Waltenberg K, Bodorkos S, Armstrong R & Fu B (2018) Mid- to lower-crustal architecture of the northern Lachlan and southern Thomson orogens: evidence from O–Hf isotopes. *Australian Journal of Earth Sciences*: 1-26.

Wark DA (1991) Oligocene ash flow volcanism, northern Sierra Madre Occidental: Role of mafic and intermediate-composition magmas in rhyolite genesis. *Journal of Geophysical Research: Solid Earth,* 96 (B8): 13389-13411.

Watson EB & Harrison TM (1983) Zircon saturation revisited: temperature and composition effects in a variety of crustal magma types. *Earth and Planetary Science Letters,* 64 (2): 295-304.

Whalen JB, Currie KL & Chappell BW (1987) A-type granites: geochemical characteristics, discrimination and petrogenesis. *Contributions to Mineralogy and Petrology,* 95 (4): 407-419.

Wilcox RE & Poldervaart A (1958) Metadolerite dike swarm in Bakersville-Roan mountain area, North Carolina. *Geological Society of America Bulletin*, 69 (11): 1323-1368.
Wollenberg HA & Smith AR (1987) Radiogenic heat production of crustal rocks: An assessment based on geochemical data. *Geophysical Research Letters*, 14 (3): 295-298.
Yoder JHS & Tilley CE (1962) Origin of Basalt Magmas: An Experimental Study of Natural and Synthetic Rock Systems. *Journal of Petrology*, 3 (3): 342-532.

Figure 1

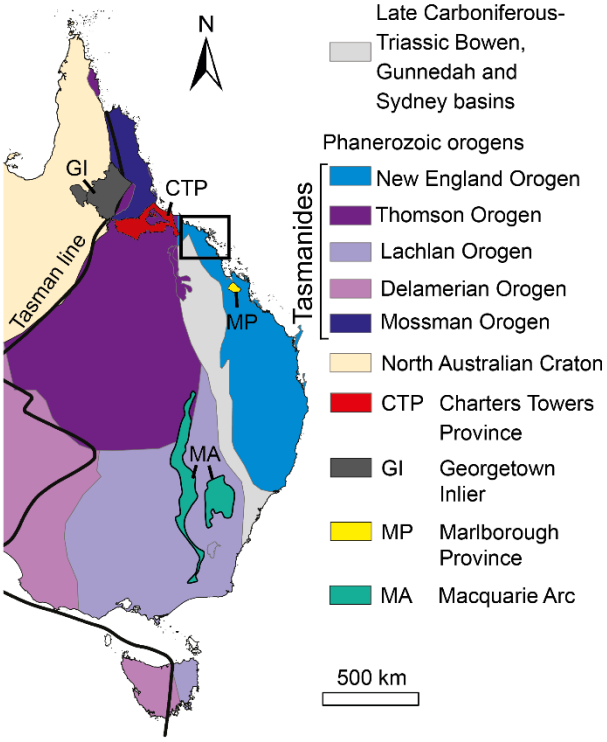
N
GI
CTP
Tasman line
MP
MA
Late Carboniferous-Triassic Bowen, Gunnedah and Sydney basins
Phanerozoic orogens
Tasmanides
New England Orogen
Thomson Orogen
Lachlan Orogen
Delamerian Orogen
Mossman Orogen
North Australian Craton
CTP Charters Towers Province
GI Georgetown Inlier
MP Marlborough Province
MA Macquarie Arc
500 km

Figure 2

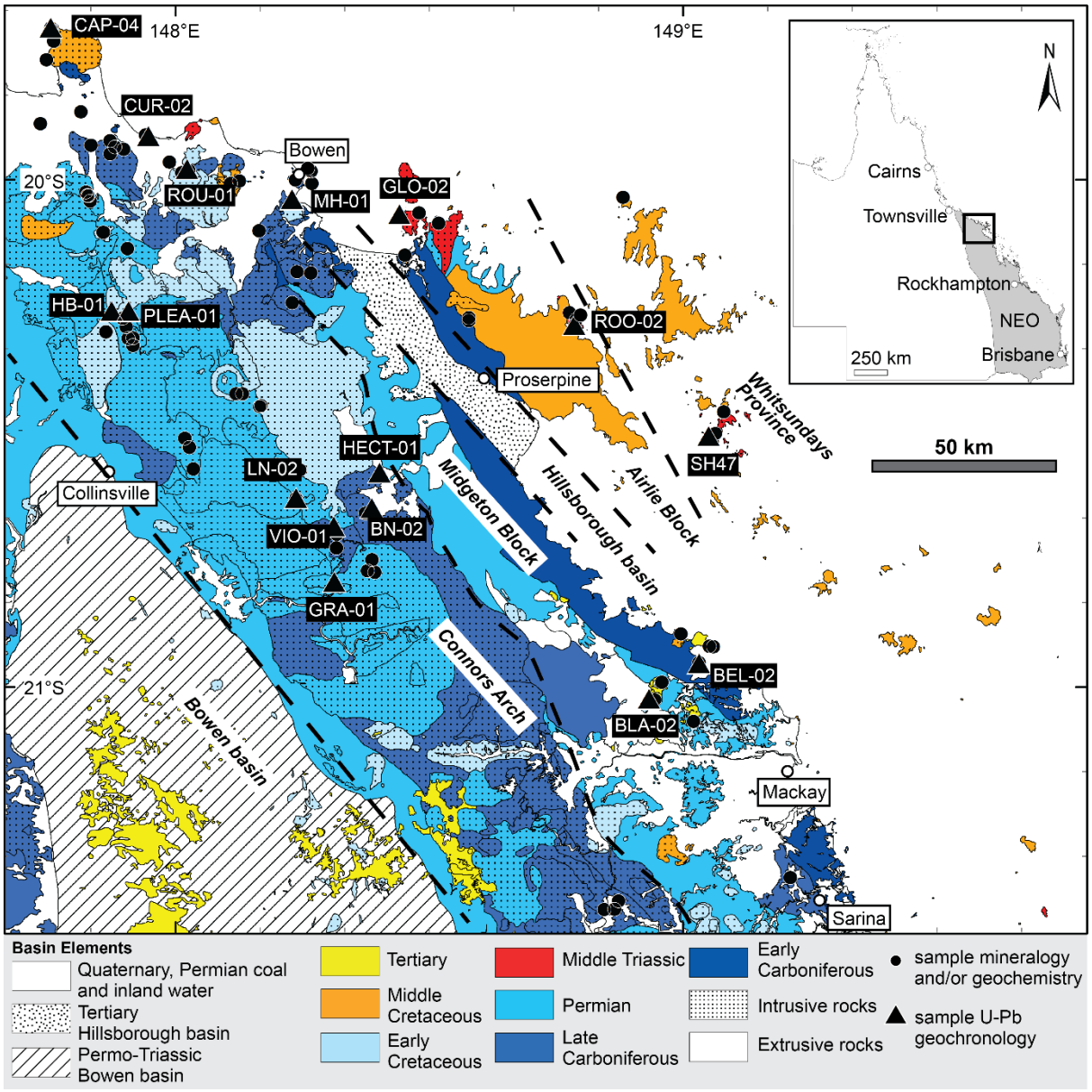
CAP-04
148°E
149°E
CUR-02
Bowen
20°S
ROU-01
MH-01
GLO-02
HB-01
PLEA-01
ROO-02
Proserpine
Whitsundays Province
SH47
50 km
HECT-01
LN-02
Collinsville
Midgeton Block
Hillsborough basin
Airlie Block
VIO-01
BN-02
GRA-01
Connors Arch
21°S
Bowen basin
BEL-02
BLA-02
Mackay
Sarina
N
Cairns
Townsville
Rockhampton
NEO
Brisbane
250 km
Basin Elements
Quaternary, Permian coal and inland water
Tertiary Hillsborough basin
Permo-Triassic Bowen basin
Tertiary
Middle Cretaceous
Early Cretaceous
Middle Triassic
Permian
Late Carboniferous
Early Carboniferous
Intrusive rocks
Extrusive rocks
sample mineralogy and/or geochemistry
sample U-Pb geochronology

Figure 3

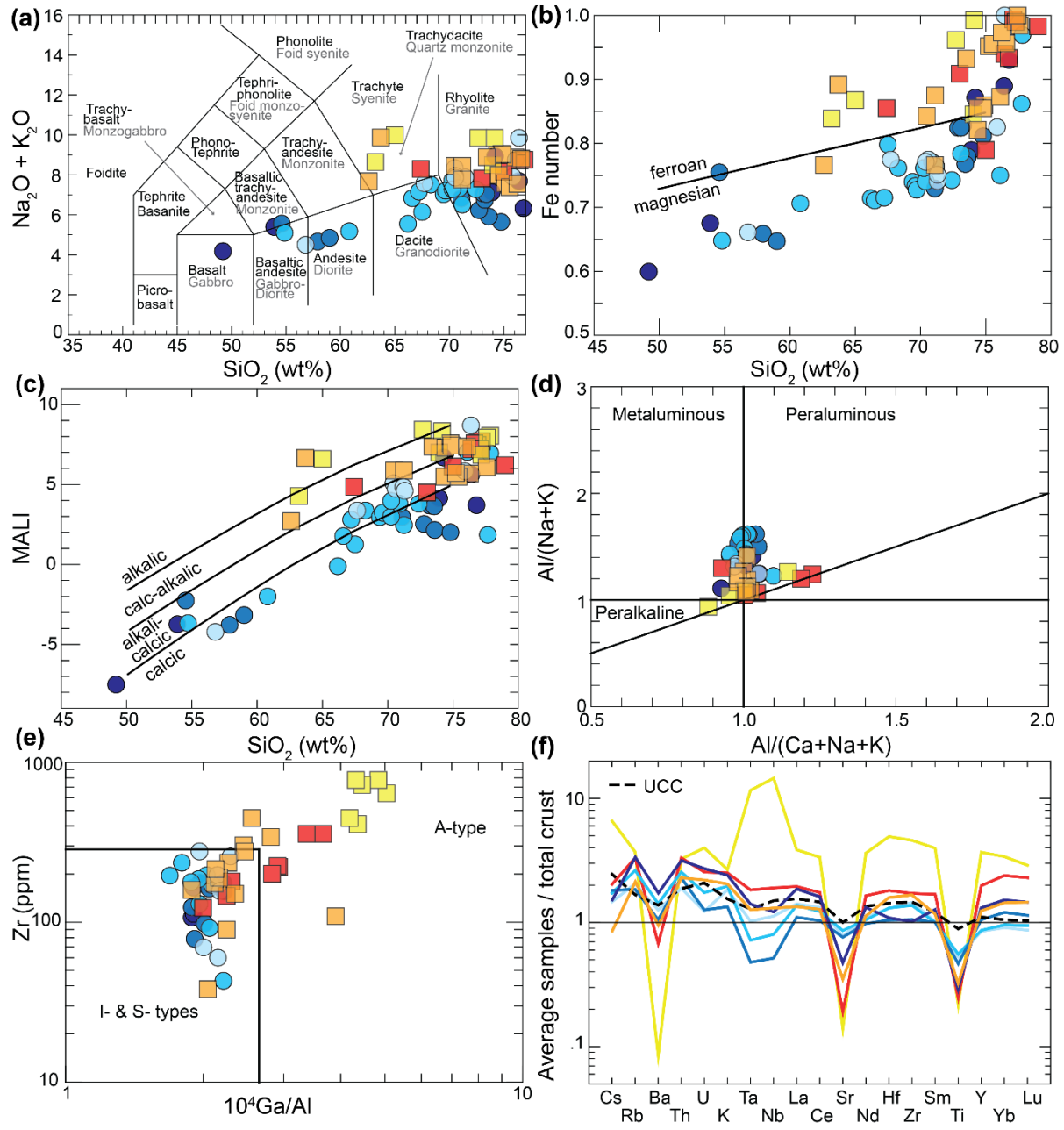
(a)
Na2O + K2O
SiO2 (wt%)
Phonolite
Foid syenite
Trachydacite
Quartz monzonite
Tephri-
phonolite
Foid monzo-
syenite
Trachyte
Syenite
Rhyolite
Granite
Trachy-
basalt
Monzogabbro
Phono-
Tephrite
Trachy-
andesite
Monzonite
Foidite
Basaltic
trachy-
andesite
Monzonite
Tephrite
Basanite
Dacite
Granodiorite
Basalt
Gabbro
Basaltic
andesite
Gabbro-
Diorite
Andesite
Diorite
Picro-
basalt
(b)
Fe number
SiO2 (wt%)
ferroan
magnesian
(c)
MALI
SiO2 (wt%)
alkalic
calc-alkalic
alkali-
calcic
calcic
(d)
Al/(Na+K)
Al/(Ca+Na+K)
Metaluminous
Peraluminous
Peralkaline
(e)
Zr (ppm)
10⁴Ga/Al
A-type
I- & S- types
(f)
Average samples / total crust
UCC
Cs Rb
Ba Th
U K
Ta Nb
La Ce
Sr Nd
Hf Zr
Sm Ti
Y Yb
Lu
Group 2
Tertiary
Middle Cretaceous
Middle Triassic
Group 1
Early Cretaceous
Permian
Late Carboniferous
Early Carboniferous
Group 2
Tertiary (n=6)
Middle Cretaceous (n=14)
Middle Triassic (n=8)
Group 1
Early Cretaceous (n=5)
Permian (n=6)
Late Carboniferous (n=7)
Early Carboniferous (n=3)

Figure 4

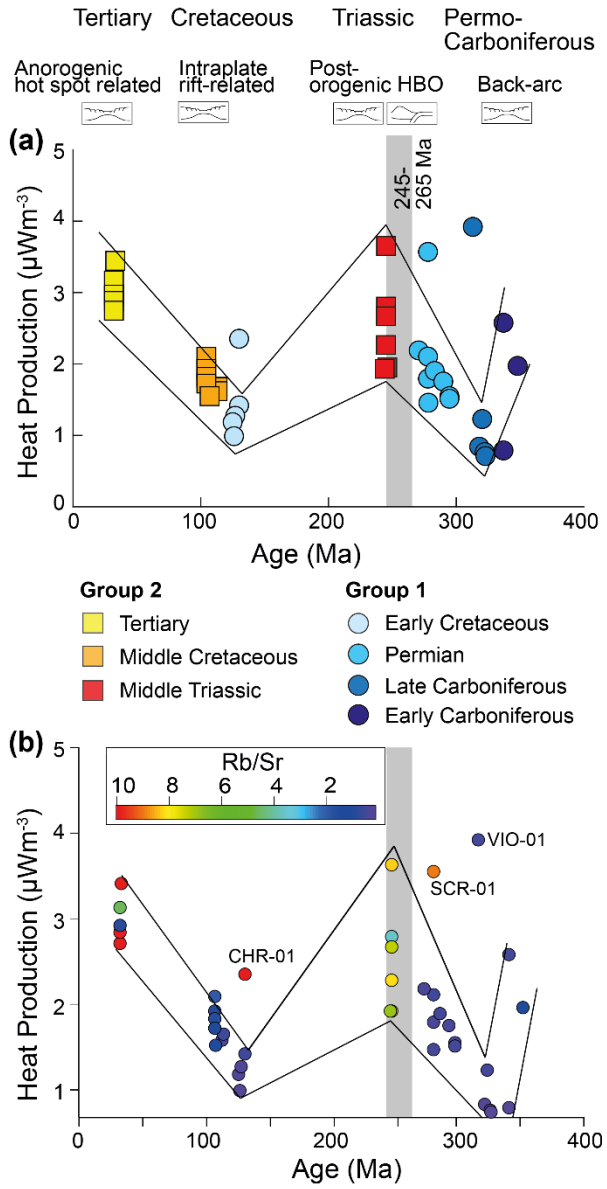
Tertiary
Cretaceous
Triassic
Permo-Carboniferous
Anorogenic hot spot related
Intraplate rift-related
Post-orogenic HBO
Back-arc
(a)
245-265 Ma
Heat Production (μWm-3)
Age (Ma)
Group 2
Tertiary
Middle Cretaceous
Middle Triassic
Group 1
Early Cretaceous
Permian
Late Carboniferous
Early Carboniferous
(b)
Rb/Sr
10 8 6 4 2
VIO-01
SCR-01
CHR-01
Heat Production (μWm-3)
Age (Ma)

Figure 5

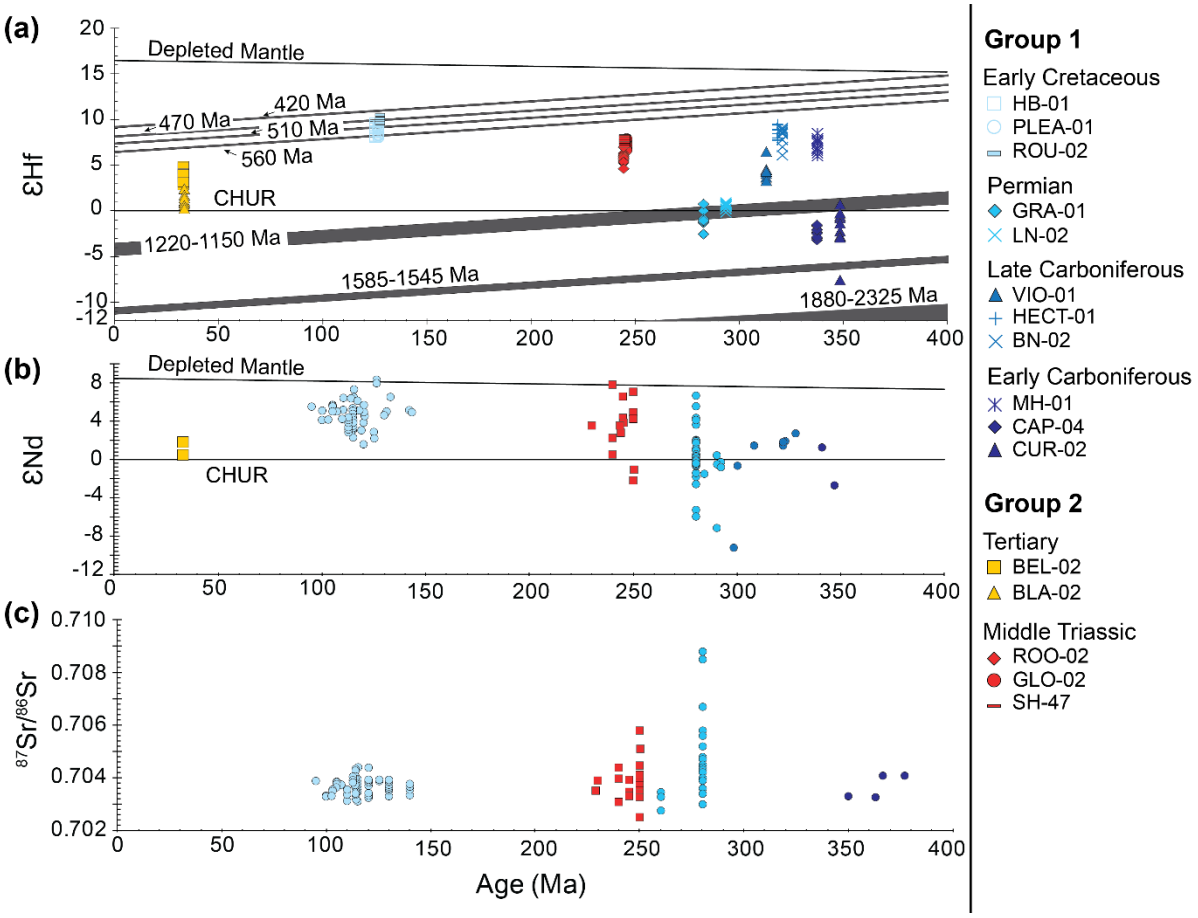
(a)
Depleted Mantle
420 Ma
470 Ma
510 Ma
560 Ma
CHUR
1220-1150 Ma
1585-1545 Ma
1880-2325 Ma
εHf
(b)
Depleted Mantle
CHUR
εNd
(c)
87Sr/86Sr
Age (Ma)
Group 1
Early Cretaceous
HB-01
PLEA-01
ROU-02
Permian
GRA-01
LN-02
Late Carboniferous
VIO-01
HECT-01
BN-02
Early Carboniferous
MH-01
CAP-04
CUR-02
Group 2
Tertiary
BEL-02
BLA-02
Middle Triassic
ROO-02
GLO-02
SH-47

Figure 6

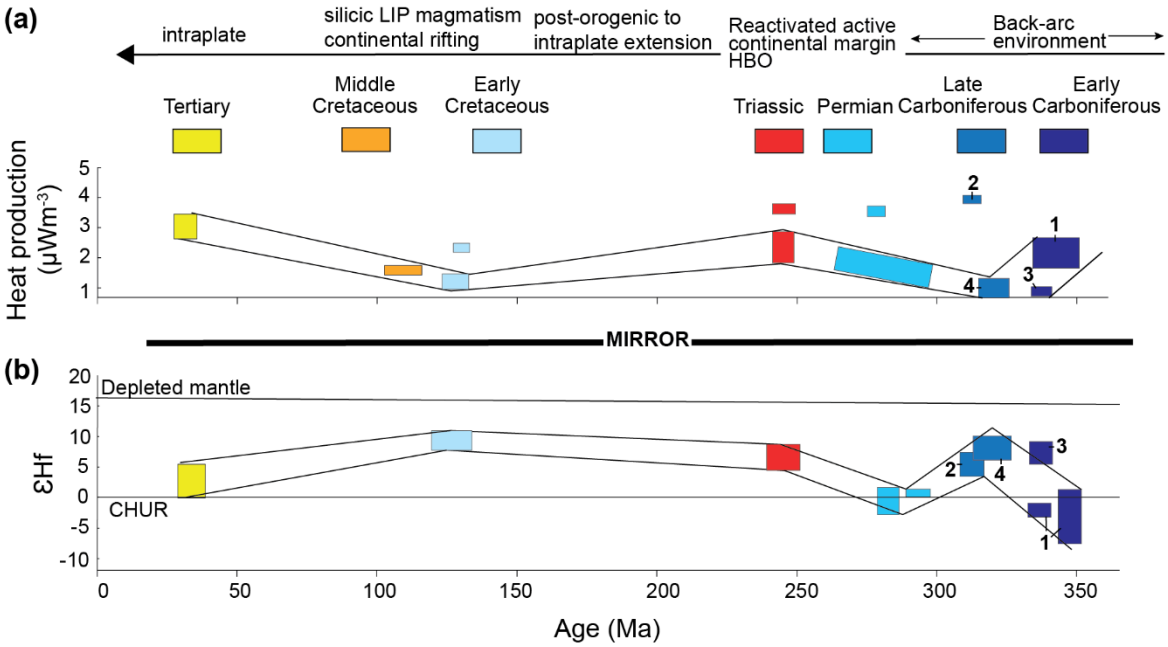
(a)
intraplate
silicic LIP magmatism
continental rifting
post-orogenic to
intraplate extension
Reactivated active
continental margin
HBO
Back-arc
environment
Tertiary
Middle
Cretaceous
Early
Cretaceous
Triassic
Permian
Late
Carboniferous
Early
Carboniferous
Heat production
(μWm-3)
MIRROR
(b)
Depleted mantle
εHf
CHUR
Age (Ma)

Figure 7

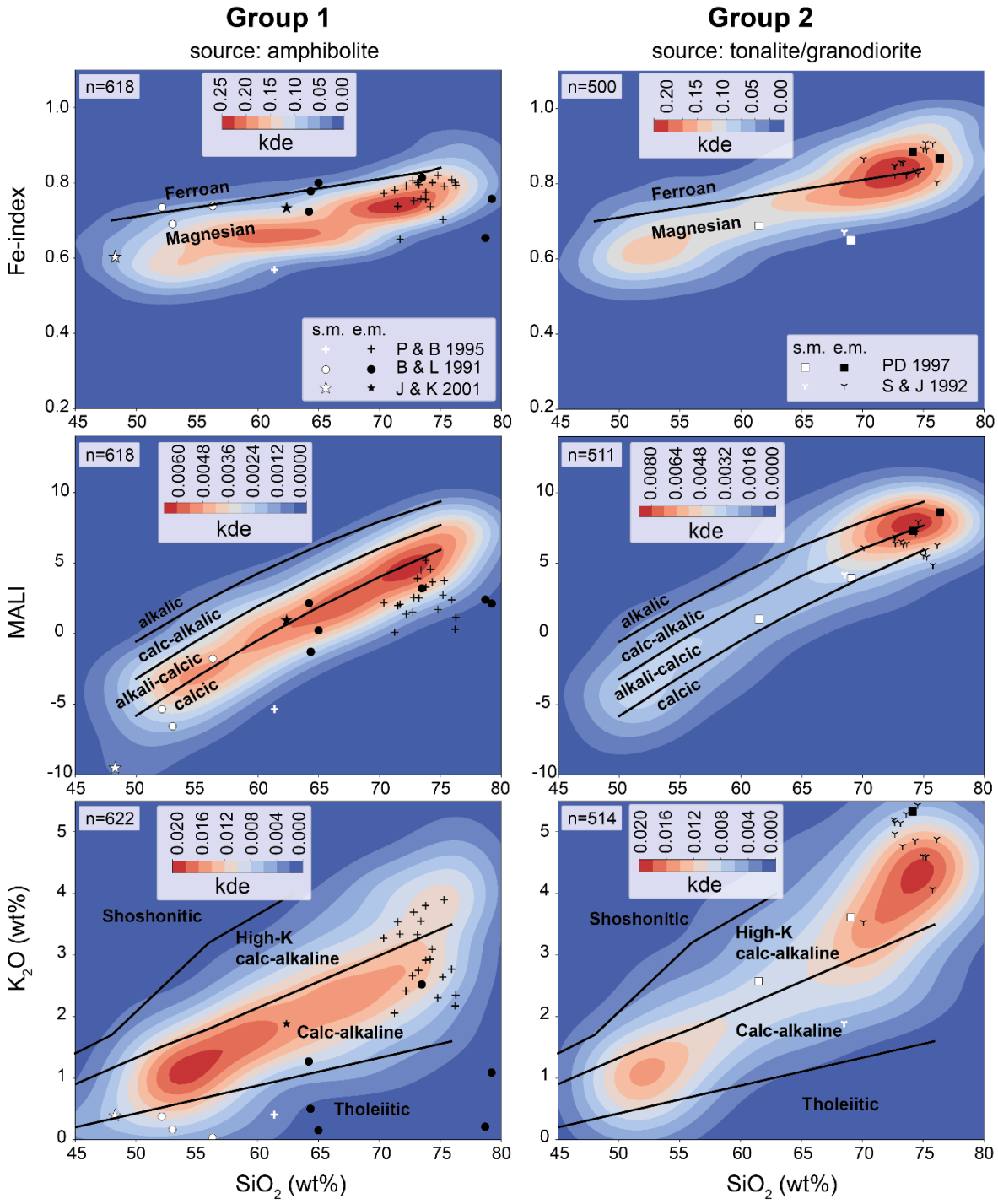
Group 1
source: amphibolite
Group 2
source: tonalite/granodiorite
n=618
n=500
n=618
n=511
n=622
n=514
kde
Ferroan
Magnesian
s.m. e.m.
P & B 1995
B & L 1991
J & K 2001
PD 1997
S & J 1992
Fe-index
MALI
alkalic
calc-alkalic
alkali-calcic
calcic
K_2O (wt%)
Shoshonitic
High-K calc-alkaline
Calc-alkaline
Tholeiitic
SiO_2 (wt%)

Figure 8

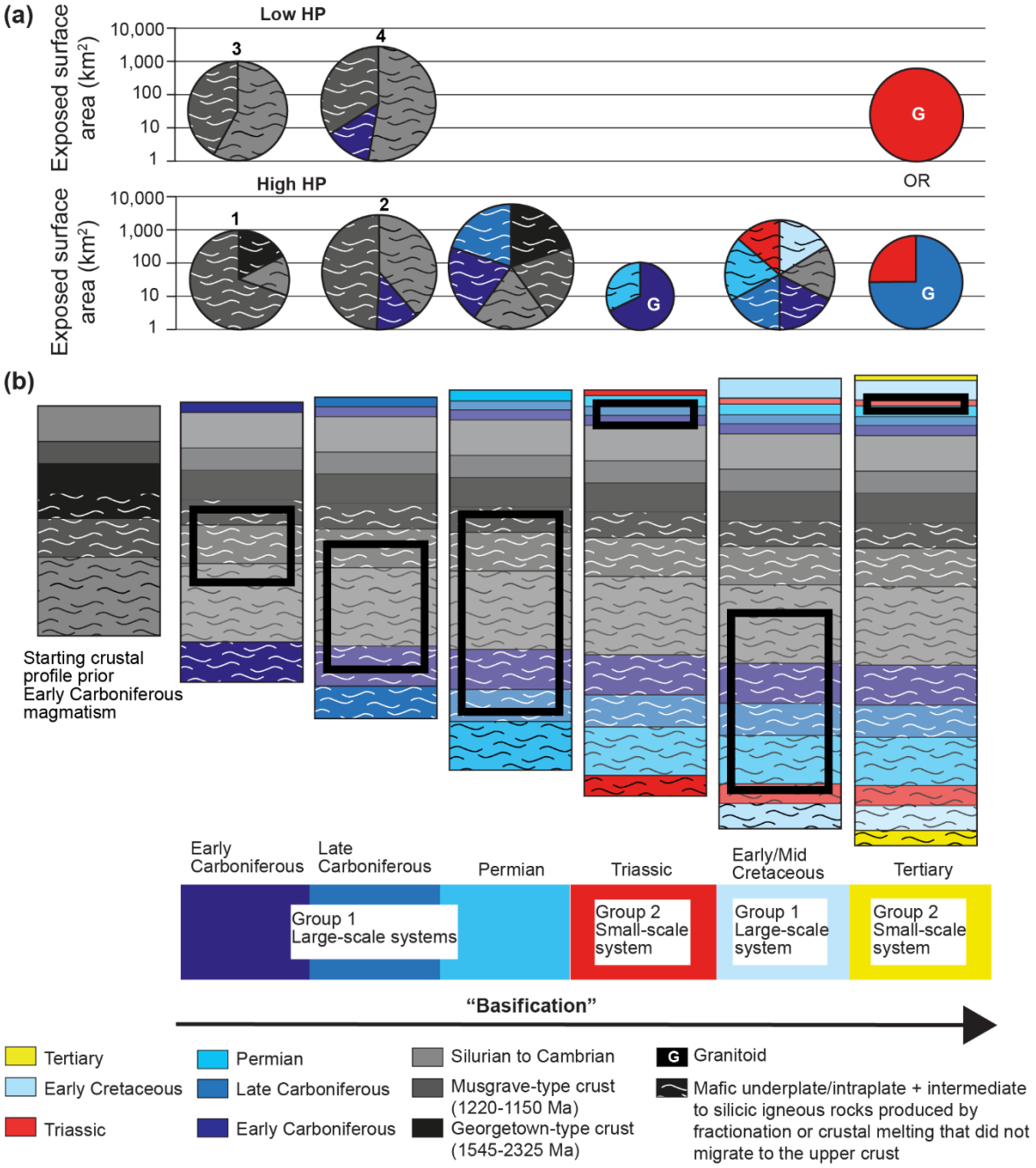
(a)
Low HP
Exposed surface area (km²)
10,000
1,000
100
10
1
3
4
G
OR
High HP
1
2
G
G
(b)
Starting crustal profile prior Early Carboniferous magmatism
Early Carboniferous
Late Carboniferous
Permian
Triassic
Early/Mid Cretaceous
Tertiary
Group 1 Large-scale systems
Group 2 Small-scale system
Group 1 Large-scale system
Group 2 Small-scale system
"Basification"
Tertiary
Early Cretaceous
Triassic
Permian
Late Carboniferous
Early Carboniferous
Silurian to Cambrian
Musgrave-type crust (1220-1150 Ma)
Georgetown-type crust (1545-2325 Ma)
G Granitoid
Mafic underplate/intraplate + intermediate to silicic igneous rocks produced by fractionation or crustal melting that did not migrate to the upper crust

Figure 9

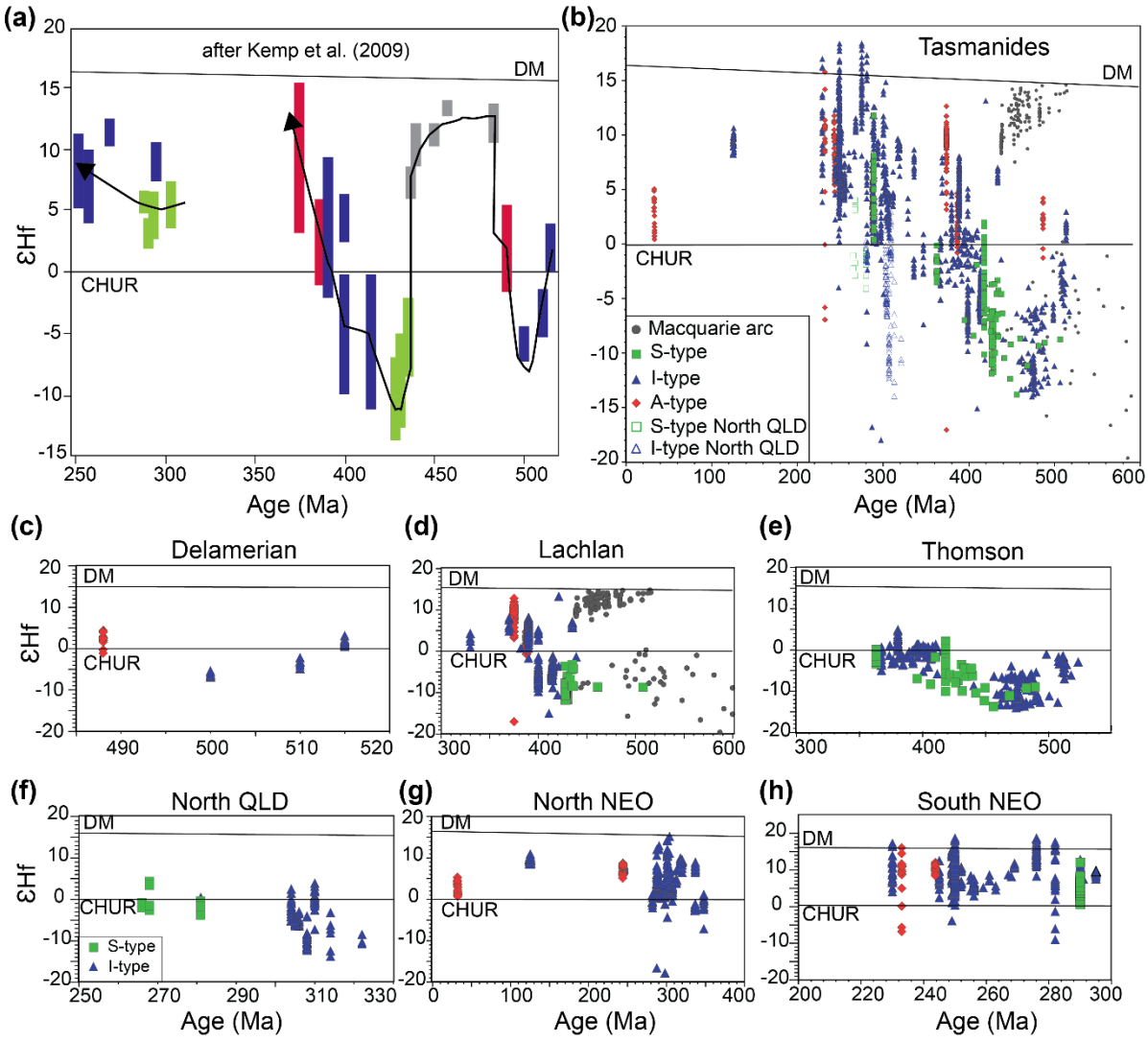
(a)
after Kemp et al. (2009)
DM
CHUR
εHf
Age (Ma)
(b)
Tasmanides
DM
CHUR
Macquarie arc
S-type
I-type
A-type
S-type North QLD
I-type North QLD
Age (Ma)
(c)
Delamerian
(d)
Lachlan
(e)
Thomson
(f)
North QLD
S-type
I-type
(g)
North NEO
(h)
South NEO

Figure 10

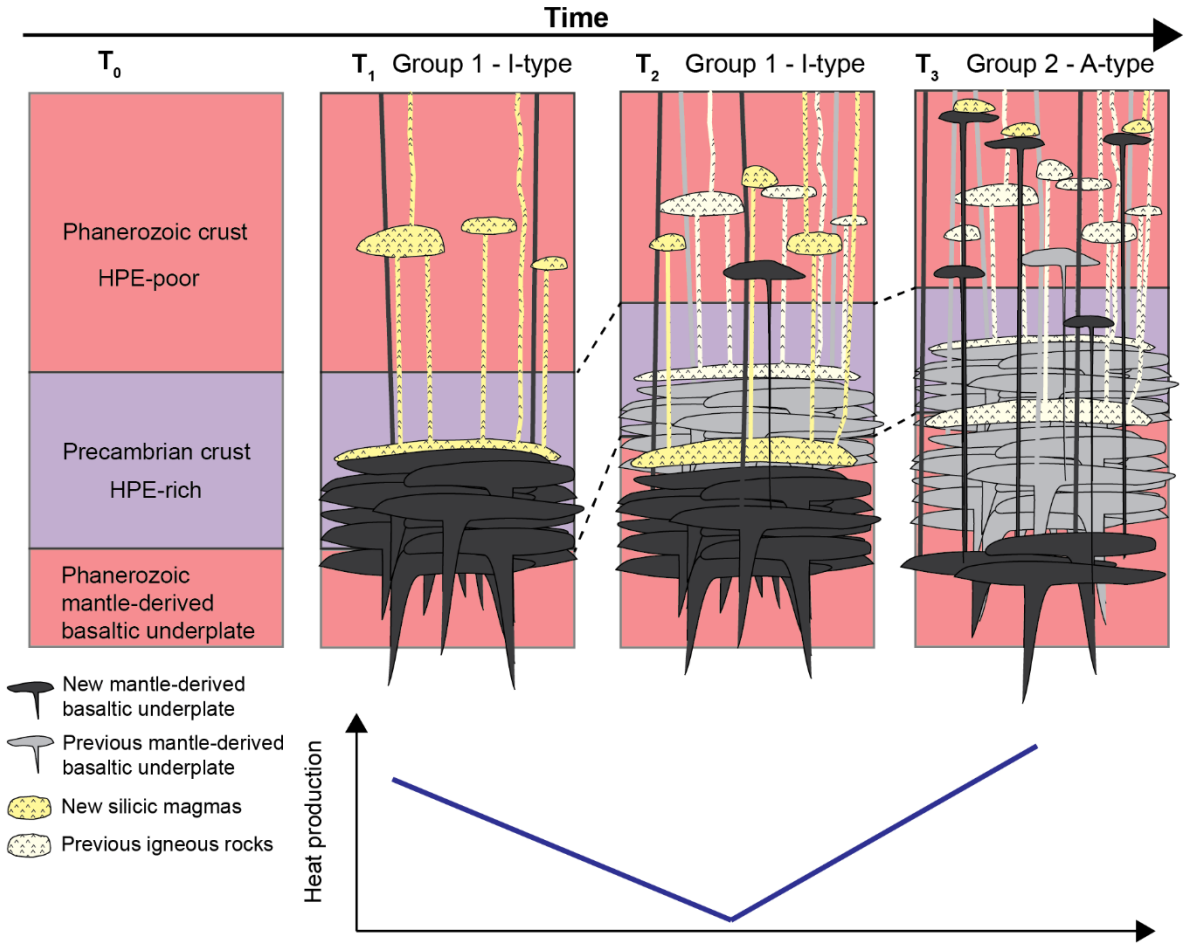
Time
T0
T1 Group 1 - I-type
T2 Group 1 - I-type
T3 Group 2 - A-type
Phanerozoic crust
HPE-poor
Precambrian crust
HPE-rich
Phanerozoic
mantle-derived
basaltic underplate
New mantle-derived
basaltic underplate
Previous mantle-derived
basaltic underplate
New silicic magmas
Previous igneous rocks
Heat production

Table 1. List of Phanerozoic igneous events in Queensland.

Time Period	Age range (Ma)	General Composition	Tectonic setting	Orogen	In the study area (Y/N)
Late Cretaceous-Tertiary	80-0	Mafic alkaline (weakly bimodal) A-type	Intraplate (hotspot)		Y
Cretaceous[1]	140-95	Silicic to bimodal, I- to A-type	Intraplate (Large Igneous Province)	Whitsundays Silicic Large Igneous Province	Y
Jurassic	168-150	Bimodal, I- to A-type	Intraplate to rift		N
Late Triassic	230-210	Silicic to bimodal A-type	Post-orogenic extension to intraplate	New England Orogen	N
Middle Triassic	245-235	Predominantly intermediate, I-type	Non-collisional orogen	New England Orogen	Y[2]
Late Permian	260-250	Intermediate to silicic, I-type	Non-collisional orogen	New England Orogen	N
Early Permian	295-270	Silicic to bimodal, I- to A-type, S-type restricted to North Queensland	Back-arc to intraplate	New England & Mossman orogens, North Australian Craton	Y
Late Carboniferous	330-305	Silicic to bimodal, I-type	Back-arc to intraplate	New England & Mossman orogens, North Australian Craton	Y
Late Devonian-Early Carboniferous	360-340	Silicic to weakly bimodal, I-type	Back-arc to continental rift	New England, Mossman and Thomson orogens	Y
Early-Late Devonian	370-360	Mafic to intermediate, I-type	Continental back-arc	New England & Thomson orogens	N
Middle Devonian	385-370	Silicic to weakly bimodal, I-type	Continental arc-rift/back-arc-rift	Thomson & New England orogens	N
Early Devonian	410-395 Ma	Silicic, I- to A-type, minor S-type	Continental rift, continental back-arc	Thomson, Mossman & New England orogens, North Australian Craton	N
Late Silurian	450-420	Mafic to silicic, S- and I-type	Continental arc/back-arc	Thomson & Mossman orogens	N
Cambrian-Ordovician	540-450	Mafic to silicic, S- and I-type	Continental arc/back-arc; continental rift	Thomson & Mossman orogens	N

[1] Note that the Cretaceous is subdivided in this study into Early (145-120 Ma) and Middle Cretaceous (120-100 Ma) based on field, mineralogical and geological information. The transition is not well-defined and is between 120 and115 Ma; [2] Middle Triassic rocks from this study are more silicic, A-type and most similar to Late Triassic igneous rocks to the South in the NEO.

Table 2. LA-ICP-MS U-Pb zircon age summary; Weighted mean ages (uncertainties are 2σ and internal/external). Ages below 1000 Ma are $^{206}Pb/^{238}U$ ages, and ages above 1000 Ma are $^{207}Pb/^{206}Pb$ ages.

Sample		Total N	N conc.	Emplacement age (Ma) +/-int./ext.	MSWD/Probability; N	Other ages (Ma) *	MSWD; Probability; N
Tertiary (35-30 Ma)							
BEL-02	Non-devitrified A-type obsidian with fayalite and embayed quartz phenocrysts	43	33	**33.23+/-0.29/0.35**	0.46/0.996; n=33	-	-
BLA-02	Medium-grained biotite A-type granodiorite	61	25	**34.34+/-0.70/0.73**	1.9/0.006; n=24	~248.8 Ma	n=1
Middle Cretaceous (120-100 Ma)[1]							
CUSA-004	Biotite leucomonzogranite	32	13	**104.4+/-1.6**	1.5/0.13; n=13	-	-
HAB1	Granite	39	26	**118.5+/-2.1**	2.4/0.000; n=25	-	-
Early Cretaceous (145-120 Ma)							
HB-01	Fine to medium-grained biotite-hornblende I-type granodiorite to monzogranite	66	47	**123.66+/-0.57/0.95**	0.94/0.58; n=40	129.7+/-1.5	1.04/0.40; n=7
ROU-02	Medium-grained biotite-hornblende I-type granodiorite	67	30	**125.0+/-1.1/1.3**	2.0/0.001; n=29	~136.5	n=1
PLEA-01	Medium-grained biotite-hornblende I-type monzogranite	80	52	**126.38+/-0.79/1.11**	2.3/0.000; n=51	~137.8	n=1
Middle Triassic (245-235 Ma)							
ROO-02	Devitrified flow-banded A-type rhyolite	48	45	**245.1+/-1.0/1.8**	0.66/0.96; n=44	~283	n=1
GLO-02	Coarse-grained biotite-hornblende I-type granodiorite	46	34	**245.3+/-1.4/2.1**	1.2/0.16; n=32	~260; ~265	n=1; n=1
SH47	Coarse-grained A-type alkali-feldspar granite	47	41	**246.3+/-1.2/1.9**	0.76/0.82; n=31	~261	n=1
Permian (295-265 Ma)							
GRA-01	Fine to medium-grained biotite-hornblende I-type monzogranite	56	47	**280.9+/-1.4/2.2**	1.8/0.001; n=45	~298; ~311	n=1; n=1
LN-02	Fine to medium-grained biotite-hornblende I-type granodiorite	57	57	**291.0+/-1.6/2.4**	3.0/0.000; n=45	309.1+/-2.2 331+/-51 ~377; ~439	0.69/0.68; n=8 2.2/0.13; n=2 n=1; n=1
Late Carboniferous (330-305 Ma)							
HECT-01	Fine to medium-grained biotite-riebeckite I-type granodiorite	55	32	**309.6+/-2.7/3.3**	1.4/0.16; n=11	322.7+-1.8 ~337; ~357	0.68/0.82; n=17 n=1; n=1
VIO-01	Medium-grained hornblende-biotite I-type monzogranite	73	53	**313.1+/-1.4/2.4**	2.0/0.000; n=49	336+/-49 ~356	2.3/0.13; n=2 n=1
BN-02	Fine to medium-grained biotite-riebeckite I-type granodiorite	64	33	**318.8+/-2.1/2.9**	2.1/0.003; n=22	342.8+/-3.8	0.40/0.81; n=5
Early Carboniferous (370-330 Ma)							
MH-01	Fine to medium-grained biotite I-type granodiorite	60	30	**333.0+/-2.0/2.9**	1.6/0.047; n=20	246.2+/-2.5** 350.6+/-4.4 ~414; ~3320	0.081/0.97; n=4 1.13/0.32; n=3 n=1; n=1
CAP-04***	Coarse-grained biotite I-type granodiorite	82	61	**336.2+/-1.4/2.5**	1.2/0.17; n=37	349.0+/-2.5 ~389; ~415 ~450; ~461; ~473	0.92/0.50; n=9 n=1; n=1 n=1; n=1; n=1
CUR-02	Fine-grained biotite-hornblende I-type syenogranite	52	41	**347.3+/-1.6/2.7**	1.5/0.030; n=30	374.1+/-4.6 ~411 471+/-11 ~550; ~1220	0.50/0.61; n=3 n=1 2.2/0.089; n=4 n=1; n=1

N is number of analyses; Conc. is concordant

+/-int./ext. is internal uncertainty/external uncertainty

[1] Unpublished data from Anderson (2016) for CUSA-004 (Cape Upstart granite), and Resende de Andrade (pers. com. 2015) for HAB1 (Hayman granite)

* Younger or inherited age populations; internal uncertainties

** This younger age is in agreement with other ages obtained from Triassic igneous rocks and is interpreted to have been affected by Pb loss in the Triassic.

*** Cape Upstart is a Middle Cretaceous intrusion (104.4 -104.8 Ma; Anderson, 2016), and the granite analysed here at the northern tip of Cape Upstart corresponds to the country rock and is of Early Carboniferous age.

Table 3. Summary of mineralogical and compositional characteristics focussing on high-silica igneous rocks from all tectonomagmatic events in the Bowen-Mackay area.

	→ Time						
	Group 1			**Group 2**	**Group 1**	**Group 2**	
	Early Carboniferous	**Late Carboniferous**	**Permian**	**Triassic**	**Early Cretaceous**	**Middle Cretaceous**	**Tertiary**
Exposed surface area within study area (km^2)	1073	3135	6413	119	1672	1024[1]	695
Field characteristics	Magma mingling	foliation	Whalebacks; large boulders	Red diagnostic colour	None	Pegmatitic patches; miarolitic cavities	None
Microgranular enclaves		Common		None	Common	Rare	Some
Rock type/granitic composition	Essentially extrusive rocks / Granodiorite to syenogranite	Essentially intrusive rocks / Granodiorite to monzogranite	Both intrusive and extrusive rocks / Granodiorite to monzogranite	Essentially intrusive rocks / Syenogranite to alkali-feldspar granite	Essentially intrusive rocks / Granodiorite to monzogranite	Essentially extrusive rocks / Monzogranite to syenogranite	Essentially extrusive rocks / Granodiorite to alkali-feldspar granite
Magnetic susceptibility (for SiO_2>70wt%; 10^{-3} SI)	9-17	0-23	2-22	<1	0-21	7-19	<3
I-, S-, A-type		I		(I to) A	I	I to A	A
Mineral proportion	↑ Plg, Bt & Hb; ↓ Afs			↓ Plg, Bt & Hb; ↑ Afs	↑ Plg, Bt & Hb, ↓ Afs	↓ Plg, Bt & Hb; ↑ Afs	
Plagioclase	High An (An05-60)			No Ca detected with EDS	High An (An10-40)	Low An (An3-26)	-
Biotite	High Mg# (20-50)			Low Mg# (<20)	High Mg# (20-50)	Low Mg# (<30)	
Plagioclase texture	Zoned and resorbed to rounded cores			Unzoned; no resorbed cores	Zoned and resorbed to rounded cores	Unzoned; no resorbed cores	
Titanite	Present			Only present in the less silicic igneous rocks	Present	Present	None
Accessory minerals	Common accessory minerals [2]			Some common[2] + Exotic[3] accessory minerals	Common accessory minerals [2]	Some common[2] + Exotic[3] accessory minerals	
T_{Zrsat}	Moderate (700-850ºC)			High (750-900ºC)	Moderate (700-850ºC)	High (750-900ºC)	High (850-950 ºC)
Geochemical character	Bimodal			silicic	intermediate	bimodal	bimodal
MALI	High (>4)	Low (<4)	Low (<4)	High (>5)	High (>4)	High (>5)	High (>7)
Ferroan/Magnesian	Magnesian to ferroan	Magnesian	Magnesian	Ferroan	Magnesian	Ferroan	Ferroan
Trace element characteristics	Low MREE, HREE, Zr and Hf, and high Ba, Sr and Ti			high MREE, HREE, Zr and Hf, and low Ba, Sr and Ti	Low MREE, HREE, Zr and Hf, and high Ba, Sr and Ti	high MREE, HREE, Zr and Hf, and low Ba, Sr and Ti	high MREE, HREE, Zr and Hf, and low Ba, Sr and Ti
Sr/Y	Moderate to High ~10-30			Low <5	Moderate to High ~10-25	Low <10	Low <5
Eu/Eu*	High >0.5			Moderate 0.1 to 0.5	High >0.5	Moderate 0.3 to 0.7	Low <0.2
T_{Tiz}	600-900 ºC	650-940 ºC	650-800 ºC	620-750 ºC	650-850 ºC	-	600-800 ºC
Ce/Ce* zircon	6-875	9-400	15-720	5-210	8-390	-	5-115

[1]Outcropping Middle Cretaceous igneous rocks are not significant in the study area but as demonstrated by Bryan et al. (2012), a large proportion has been eroded and estimates indicate voluminous magmatism at this time.
Abbreviations are: Plg, plagioclase; Bt, biotite; Hb, hornblende; Afs, alkali-feldspar; T_{Zrsat}, zircon saturation temperature; T_{Tiz}, Ti in zircon temperature
[2]Common accessory minerals: thorite/huttonite, monazite, cheralite, allanite, xenotime, apatite, titanite, zircon
[3]Exotic accessory minerals: Parisite-Nd, samarskite, uranoan Zr-rich thoriopyrochlore, fluocerite, chevkinite, fluorite

Table 4. Scale of magmatism for Group 1 and Group 2 igneous rocks[1]

Igneous event (age/age range)	**Exposed surface area within study Area (km^2)**	**% of study area (22,390 km^2)**	**% of exposed igneous rocks (14,131 km^2)**
Tertiary	695	3.1	4.9
Middle Cretaceous	1,024	4.6	7.2
Early Cretaceous	1,672	7.5	11.8
Triassic	119	0.5	0.8
Permian	6,413	28.6	45.4
Late Carboniferous	3,135	14.0	22.2
Early Carboniferous	1,073	4.8	7.6
Group 1	12,293	54.9	61.5
Group 2	1,838	8.2	9.2

[1] This is based on Figure 2 and does not include the ocean surface.

Table 5. Nature of igneous crustal sources. In bold are dominant crustal sources as illustrated in the pies of Figure 8.

	Group	1	1	1	2	1	2
	Igneous event	Early Carboniferous	Late Carboniferous	Permian	Triassic	Early Cretaceous	Tertiary
Crustal Source Ages	Georgetown-type (~1900 Ma)	**X**		X			
	Musgrave-type (~1200 Ma)	**X**	X	X			
	Charters Towers-type (~500-420 Ma)	X	X	X		X	
	Carboniferous (~360-300 Ma)		X	X	**X**^{S}	X	X^{S}
	Permian (~290-270 Ma?)				X^{S}	X	
	Triassic (~250-230 Ma)					X	X^{S}
	Early Cretaceous (~130-140 Ma)					X	
Evidence		T_{2DM}: 700 to 870 Ma (MH-01); 1180-1660 Ma (CAP-04; CUR-02) ZI: Mesoproterozoic, Ordovician and Silurian	T_{2DM}: 650-1000 Ma ZI: Cambro-Silurian and Early Carboniferous	T_{2DM}: 1130-1320 Ma ZI: Archean, Late to Early Mesoproterozoic, Cambro-Silurian and Carboniferous [1]	T_{2DM}: 660-870 Ma; similar to the most radiogenic Carboniferous granitoids. High HPE & silica contents ZI: Permian	T_{2DM}: 430-580 Ma ZI: Late Cambrian to Cretaceous	T_{2DM}: 680-950 Ma; similar to the Triassic and the most radiogenic Carboniferous granitoids. High HPE & silica contents ZI: Triassic, Silurian to Precambrian in granulitic xenoliths at the northern tip of the Bowen Basin [2]

[1] Data from this study, Withnall et al (2009) and Cross et al (2012)
[2] Zircon inheritance in granulitic xenoliths from Allen & Williams (1998)
[S] source is supracrustal. Partial melting of a granitoid rather than mantle-derived magmas added into the crust.
ZI: Zircon inheritance